is necessary, but because of the early mesodermal defects already described, these knockout embryos lack a paraxial mesoderm, which prevents any analysis of somitogenesis. We therefore adopted a strategy that utilized chimera analysis. As we have reported previously, the early embryonic lethality of a Mesp1/Mesp2 double knockout is rescued by the presence of wild-type cells in a chimeric embryo, but the double-null cells cannot contribute to the cardiac mesoderm (Kitajima et al., 2000). This analysis, however, focused only on early heart morphogenesis and did not investigate the behavior of Mesp1/Mesp2 double-null cells in somitogenesis. In this report, we focus upon somitogenesis and compare two types of chimeras using either Mesp1/Mesp2 double-null cells or Mesp2-null cells to investigate Mesp1 function during somitogenesis.

Another purpose of our chimera experiments was to elucidate the cell autonomy of Mesp functions. In the process of somite formation, mesenchymal cells in the PSM initially undergo epithelialization at the future segment boundary, independently of the already epithelialized dorsal or ventral margin of the PSM (Sato et al., 2002). Epithelial somite formation is disrupted in the Mesp2-null embryo, indicating that Mesp2 is required for epithelialization at the segment boundary. Although Mesp products are nuclear transcription factors and their primary functions must therefore be cell autonomous (transcriptional control of target genes), it is possible that the roles of Mesp2 in epithelialization are mediated by the non-cell autonomous effects of target genes. We therefore asked whether the defects in Mesp2-null cells during epithelialization could be rescued by the presence of surrounding wild-type cells. Additionally, we would expect to find that the role of Mesp2 in establishing rostro-caudal polarity is rescued in a similar way.

Our analysis suggests that Mesp1 and Mesp2 have redundant functions and are both cell-autonomously involved in the epithelialization of somitic mesoderm. In addition, our results highlight some non-cell autonomous effect of Mesp2-null and Mesp1/Mesp2-null cells.

Materials and methods

Generation of chimeric embryos

As described previously (Kitajima et al., 2000), chimeric embryos were generated by aggregating 8-cell embryos of wild-type mice (ICR) with those of mutant mice that were genetically marked with the *ROSA26* transgene (Zambrowicz et al., 1997). Mesp1/Mesp2 double-null embryos were generated by crossing *wko-del (+/–)* and *Mesp1(+/–)/Mesp2(+/cre)* mice as described previously (Kitajima et al., 2000). This strategy enables us to distinguish chimeric embryos derived from homozygous embryos, which have two different mutant alleles, from those derived from heterozygous embryos. Likewise, Mesp2-null embryos were generated by crossing *P2v1(+/–)* mice (Saga et al., 1997) and *P2GFP (+/gfp)* mice (Y.S. and S.K., unpublished) that were also labeled with the *ROSA26* locus. The genotype of the chimeric embryos was determined by PCR using yolk sac DNA.

Histology, histochemistry and gene expression analysis

The chimeric embryos were fixed at 11 days postcoitum (dpc) and stained in X-gal solution for the detection of β-galactosidase activity, as described previously (Saga et al., 1999). For histology, samples stained by X-gal were postfixed with 4% paraformaldehyde, dehydrated in an ethanol series, embedded in plastic resin (Technovit 8100, Heraeus Kulzer) and sectioned at 3 μm. The methods used for gene expression analysis by in-situ hybridization of whole-mount samples and frozen sections and skeletal preparation by Alcian Blue/Alizarin Red staining were described previously (Saga et al., 1997; Takahashi et al., 2000). Probes for in-situ hybridization for *Uncx4.1* (Mansouri et al., 1997; Neidhardt et al., 1997), *Delta-like 1 (Dll1)* (Bettenhausen et al., 1995) and *Paraxis* (Burgess et al., 1995) were kindly provided by Drs Peter Gruss, Achim Gossler and Alan Rawls, respectively. A probe for *EphA4* (Nieto et al., 1992) was cloned by PCR. For detection of actin filaments, frozen sections were stained with AlexaFluor 488-conjugated phalloidin (Molecular Probes) according to the manufacturer's protocol.

Results

Possible functional redundancy and different contributions of Mesp1 and Mesp2 in somitogenesis

During somitogenesis, both *Mesp1* and *Mesp2* are expressed in the anterior PSM just prior to somite formation and their expression domains overlap (Fig. 1A). Mesp1-null embryos form morphologically normal somites and show normal rostro-caudal patterning within each somite (Fig. 1B,E-H), indicating that Mesp1 is not essential for somitogenesis. By contrast, Mesp2 is essential for both the formation and rostro-caudal patterning of somites, as Mesp2-null embryos have no epithelial somites and lose rostral half properties, resulting in caudalization of the entire somitic mesoderm (Saga et al., 1997) (Fig. 1C,D).

Although somite formation and rostro-caudal patterning is disrupted in the Mesp2-null embryo, histological differentiation into dermomyotome and sclerotome is not affected. It is noteworthy that the Mesp2-null embryo still forms disorganized dermomyotomes without forming epithelial somites (Saga et al., 1997). As *Mesp1* is expressed at normal levels in the PSM of Mesp2-null embryos (Fig. 1C,D), it is possible that Mesp1 functions to rescue some aspects of somitogenesis in the Mesp2-null embryo. In order to further clarify the contributions of both Mesp1 and Mesp2 during somitogenesis, we therefore generated chimeric embryos with either Mesp2-null cells or Mesp1/Mesp2 double-null cells and compared the behavior of mutant cells during somitogenesis (Fig. 2).

Mesp2-null cells tend to be eliminated from the epithelial somite and the dermomyotome, but can partially contribute to both of these structures

We first generated Mesp2-null chimeric embryos (*Mesp2*$^{-/-}$ with *Rosa26*: wild) to analyze cell autonomy of Mesp2 function during somitogenesis. The control chimeric embryo (*Mesp2*$^{+/-}$ with *Rosa26*: wild) showed normal somitogenesis and a random distribution of X-gal stained cells (Fig. 3A). The Mesp2-null chimeric embryos formed abnormal somites that exhibited incomplete segmentation (Fig. 3B), but histological differentiation of dermomyotome and sclerotome was observed. Within the incomplete somite, X-gal-stained Mesp2-null cells were mainly localized in the rostral and central regions, surrounded by wild-type cells at the dorsal, ventral and caudal sides (Fig. 3B). The surrounding wild-type cells, however, did not form an integrated epithelial sheet, but consisted of several epithelial cell clusters. Such trends were more obviously observed in other sections, where wild-type cells were found to form multiple small epithelial clusters (Fig.

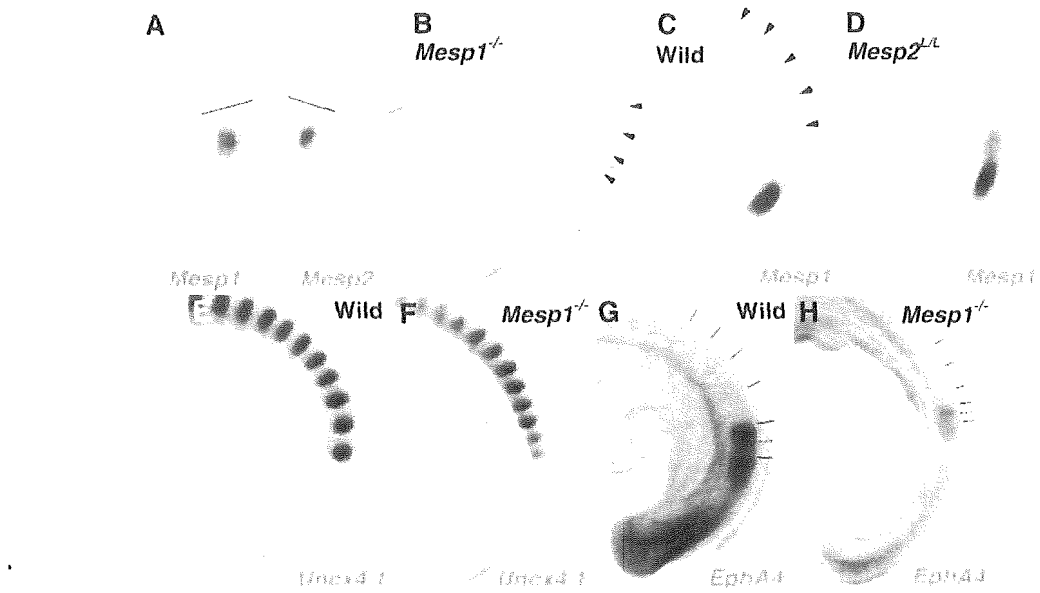

Fig. 1. *Mesp1* and *Mesp2* are co-expressed in the anterior PSM but have differing roles in somitogenesis. (A) Overlapping expression of *Mesp1* and *Mesp2* is revealed by in-situ hybridization using the left and right halves of the same embryo. The lines show most recently formed somite boundaries. (B-C) A Mesp1-null embryo (B) shows the same normal somite formation as a wild-type embryo (C). Arrowheads indicate somite boundaries. (D) In Mesp2-null embryos, no somite formation is observed but *Mesp1* is expressed at comparable levels to wild type, although its expression is anteriorly extended and blurred. (E-H) Mesp1-null embryos show normal rostro-caudal patterning of somites. (E,F) Expression of a caudal half marker, *Uncx4.1*. (G,H) Expression of a rostral half marker, *EphA4*. The lines indicate presumptive or formed somite boundaries and the dotted line indicates approximate position of somite half boundary.

3C,D). Mesp2-null cells tended to be eliminated from the epithelial clusters, although they were partially integrated into these structures (blue arrows in Fig. 3C,D). Likewise, small numbers of Mesp2-null cells were found to contribute to the dermomyotome (Fig. 3E,F). Mesp2-null cells also appeared to form the major part of the sclerotome.

Mesp2 is required for the cell-autonomous acquisition of rostral properties

We have previously demonstrated that suppression by Mesp2

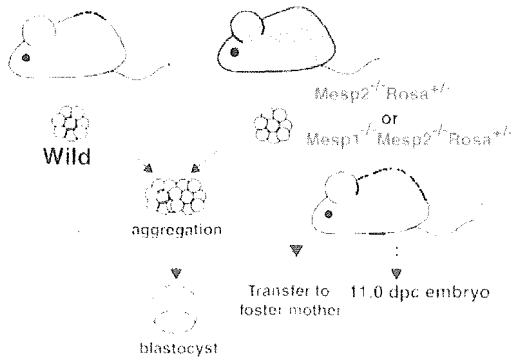

Fig. 2. Schematic representation of chimera analysis method. Either Mesp2-null or Mesp1/Mesp2 double-null embryos, genetically labeled with *Rosa* locus, were aggregated with wild-type embryos at the 8-cell stage, and the resulting chimeras were subjected to analysis at 11.0 dpc.

of the caudal genes *Dll1* and *Uncx4.1* in presumptive rostral half somites is a crucial event in the establishment of the rostro-caudal pattern of somites (Saga et al., 1997; Takahashi et al., 2000). As Mesp2-null embryos exhibit caudalization of somites, Mesp2-null cells are predicted to be unable to express rostral properties. Hence, Mesp2-null cells are expected to distribute to the caudal region of each somite where the rostro-caudal patterns are rescued by wild-type cells in a chimeric embryo. In this context, the localization of Mesp2-null cells at the rostral side was an unexpected finding. We interpret this to mean that the rostral location of Mesp2-null cells is due to a lack of epithelialization functions (see Discussion).

To examine rostro-caudal properties in Mesp2-null cells, located in the rostral side, we analyzed the expression of a caudal half marker gene, *Uncx4.1* (Mansouri et al., 1997; Neidhardt et al., 1997). Analysis of adjacent sections revealed that *lacZ*-expressing Mesp2-null cells, localized at the rostral and central portion, ectopically expressed *Uncx4.1* (Fig. 4A-D). This strongly suggests that Mesp2-null cells cannot acquire rostral properties even if surrounded by wild-type cells, and that Mesp2 function is cell-autonomously required for the acquisition of rostral properties. We also observed that the small number of Mesp2-null cells distributed mostly to the caudal end of the dermomyotome (Fig. 3E,F) and that the expression pattern of *Uncx4.1* was normal in the dermomyotome (Fig. 4E,F). In the sclerotome, *lacZ*-expressing Mesp2-null cells often distributed to the rostral side, where expression of *Uncx4.1* was abnormally elevated (Fig. 4G,H). The vertebrae of the Mesp2-null chimeric fetus showed a partial fusion of the neural arches, which was reminiscent of

Mesp2-hypomorphic fetuses (Fig. 4I,J) (Nomura-Kitabayashi et al., 2002). Fusion of proximal rib elements was also observed (Fig. 4K,L).

Mesp1/Mesp2 double-null cells cannot contribute to the formation of epithelial somites or to the dermomyotome

To address the question of whether Mesp1, in addition to Mesp2, exhibits any function during somitogenesis, we next generated Mesp1/Mesp2 double-null chimeric embryos and compared them with the Mesp2-null chimeric embryos described in the previous sections. We first performed whole-mount X-gal staining of embryos at 11 dpc. In the control chimeric embryo, the X-gal-stained Mesp1/Mesp2 double-heterozygous cells distributed randomly throughout the embryonic body, including the somite region (Fig. 5A,C). By contrast, the Mesp1/Mesp2 double-null chimeric embryo displayed a strikingly uneven pattern of cellular distribution in the somite region. The X-gal stained Mesp1/Mesp2 double-null cells were localized at the medial part of embryonic tail and were not observed in the lateral part of the somite region (Fig. 5B,D). Histological examination of parasagittal sections further revealed obvious differences in the cellular contribution to somite formation (Fig. 5E,F). In the control chimeric embryo, Mesp1/Mesp2 double-heterozygous cells distributed randomly throughout the different stages of somitogenesis (PSM, somite, dermomyotome and sclerotome; Fig. 5E). In the Mesp1/Mesp2 double-null chimeric embryo, neither the initial segment border nor epithelial somites were formed, but histologically distinguishable dermomyotome-like and sclerotome-like compartments were generated (Fig. 5F). In addition, Mesp1/Mesp2 double-null cells and wild-type cells were randomly mixed in the PSM, whereas the dermomyotome-like epithelium consisted exclusively of wild-type cells and the sclerotome-like compartment consisted mostly of Mesp1/Mesp2 double-null cells. This suggests that either Mesp1 or Mesp2 is cell-autonomously required for the formation of epithelial somite and dermomyotome. These results also indicate that PSM cells with different characteristics are rapidly sorted during somite formation.

Subsequent examination of transverse sections confirmed the elimination of Mesp1/Mesp2 double-null cells from dermomyotome (Fig. 5G,H). In the mature somite region, the wild-type dermomyotome-like epithelium was found to form the myotome (my) (Fig. 5I,J). Furthermore, the ventral part of this dermomyotome-like epithelium became mesenchymal and appeared to contribute to the dorsal sclerotome (dsc), implying that this initial dermomyotome-like epithelium actually corresponds to the epithelial somite exclusively composed of wild-type cells (Fig. 5I,J). Fluorescent phalloidin staining revealed that the apical localization of actin filaments is limited to the dorsal compartments, which are occupied by wild-type cells in the Mesp1/Mesp2 double-null chimeric embryo (Fig. 5K,L), indicating the Mesp1/Mesp2 double-null cells cannot undergo epithelialization.

It is known that the bHLH transcription factor paraxis (Tcf15 – Mouse Genome Informatics), is required for the epithelialization of somite and

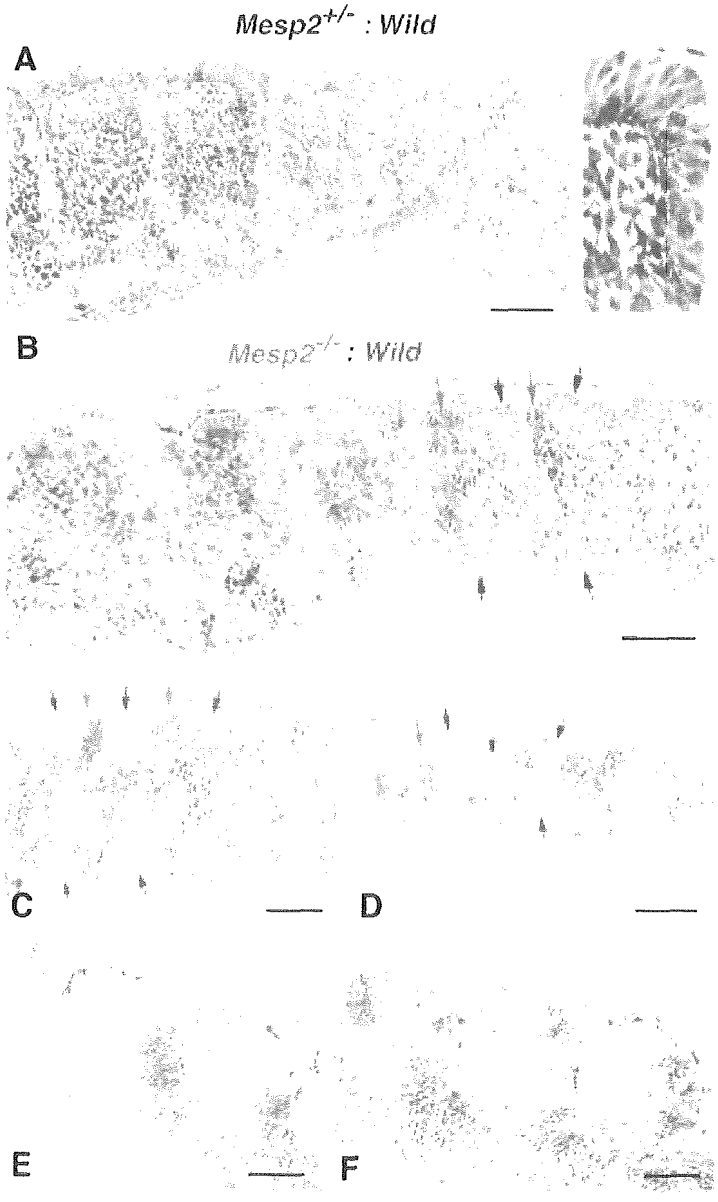

Fig. 3. Mesp2-null cells tend to be excluded from the epithelial region of the somites. (A) The control chimeric embryo undergoes normal somite formation and shows random distribution of labeled cells. The right panel is a high-power view of a somite. (B) In the Mesp2-null chimeric embryo, incompletely segmented somites are formed. Mesp2-null cells tend to be localized at the rostral and central region of these incomplete segments. Red arrows: wild-type cell clusters; blue arrows: Mesp2-null cell clusters. (C,D) Other sections indicating multiple small epithelial cell clusters (arrows). Note that Mesp2-null cells only partially contribute to the epithelial clusters (blue arrows). (E,F) A small number of Mesp2-null cells are distributed in the dermomyotome and are mostly localized at the caudal end. Scale bars: 100 μm.

dermomyotome (Burgess et al., 1995; Burgess et al., 1996). Although *Paraxis* expression is not affected in Mesp2-null embryos (data not shown), it is possible that it is influenced by the loss of both Mesp1 and Mesp2. We therefore examined the expression patterns of *Paraxis* in our Mesp1/Mesp2 double-null chimeras. In wild-type embryos *Paraxis* is initially expressed throughout the entire somite region (in both the prospective dermomyotomal and sclerotomal regions) in the anteriormost PSM and newly forming somites, and then localizes in the dermomyotomes (Burgess et al., 1995). The dorsal dermomyotomal epithelium, composed of wild-type cells, strongly expressed *Paraxis* in the chimeric embryo (Fig. 6A,B). In addition, adjacent sections revealed that *lacZ*-expressing Mesp1/Mesp2 double-null cells expressed *Paraxis* in the medial sclerotomal compartment (Fig. 6A,B, brackets). This suggests that *Paraxis* expression in the future sclerotomal region is independent of Mesp factors. However, at present we cannot exclude the possibility that the maintenance of *Paraxis* expression in the dermomyotome requires the functions of either Mesp1 or Mesp2.

Mesp1/Mesp2 double-null cells are incapable of acquiring rostral properties

To clarify the rostro-caudal properties of somites in our chimeric embryos, we examined the expression pattern of *Uncx4.1*. Control chimeric embryos exhibited a normal stripe pattern of *Uncx4.1* expression throughout the segmented somite region (Fig. 7A). By contrast, Mesp1/Mesp2 double-null chimeric embryos exhibited continuous *Uncx4.1* expression in the ventral sclerotomal region (Fig. 7B). This continuity was observed in the entire sclerotome-like compartment of the newly formed somite region and in the ventral sclerotome in the mature somite region. The caudal localization of *Uncx4.1* expression, however, was normal in the dermomyotome and the dorsal sclerotome, which consisted of wild-type cells (Fig. 5), even in Mesp1/Mesp2 double-null chimeras. This suggests that, like Mesp2-null cells, Mesp1/Mesp2 double-null cells are incapable of acquiring rostral properties. Since the mesoderm of Mesp1/Mesp2 double-null embryos lacks the expression of the major markers of paraxial mesoderm (Kitajima et al., 2000), and Mesp1/Mesp2 double-null cells do not exhibit histological features characteristic of epithelial somites in our current study, it is possible that Mesp1/Mesp2 double-null cells may lack paraxial mesoderm properties. However, the analysis of adjacent sections suggests that *lacZ*-expressing Mesp1/Mesp2 double-null cells themselves express *Uncx4.1*, a somite-specific marker (Fig. 7C,D), and they had also been found to have normal expression of *Paraxis* (Fig. 6A,B).

It is believed that the rostro-caudal pattern within somites and dermomyotomes is generated in the PSM and maintained in somites and dermomyotomes. We observed a normal rostro-caudal pattern in the dermomyotome (Fig. 7), although wild-type cells and Mesp1/Mesp2 double-null cells are mixed in the PSM (Fig. 5), of Mesp1/Mesp2 double-null chimeric embryos. As Mesp products are required for suppression of *Dll1* in the anterior PSM, a normal Dll1 stripe pattern cannot be formed if Mesp1/Mesp2 double-null cells are randomly distributed in

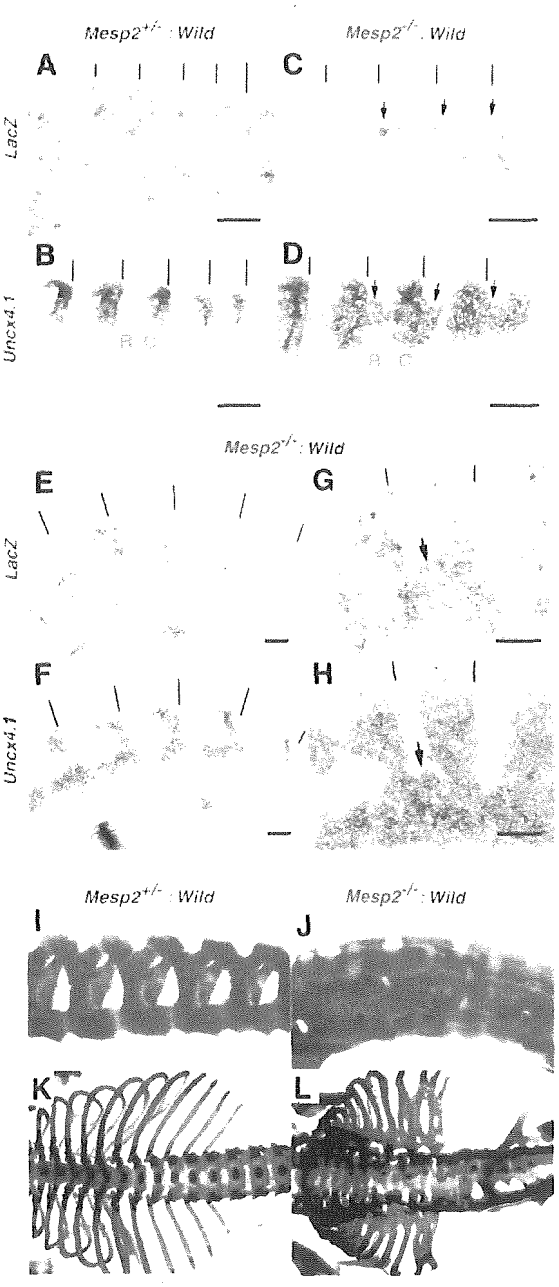

Fig. 4. Mesp2 function is cell autonomously required for rostral properties. (A-D) Expression of *lacZ* and *Uncx4.1* transcripts at the site of initial somite formation in control (A,B) and Mesp2-null (C,D) chimeric embryos. In the control, *lacZ*-expressing cells are randomly distributed and *Uncx4.1* expression is normal. In the Mesp2-null chimera, *lacZ*-expressing Mesp2-null cells at the rostral part of the incomplete segments (arrows in C) ectopically express *Uncx4.1* (arrows in D). Lines indicate somite boundaries. (E,F) In the dermomyotome, Mesp2-null cells are mostly localized at the caudal end, and the *Uncx4.1* expression pattern is normal. (G,H) In the sclerotome, the distribution of Mesp2-null cells results in expansion of *Uncx4.1* expression (arrows). (I) The control chimeric fetus shows normal vertebrae. (J) The Mesp2-null chimeric fetus exhibits partial fusion of the neural arches. (K) The control chimeric fetus shows normal ribs. (L) The Mesp2-null chimeric fetus shows proximal rib fusion. Scale bars: 100 μm. C, caudal compartment; R, rostral compartment.

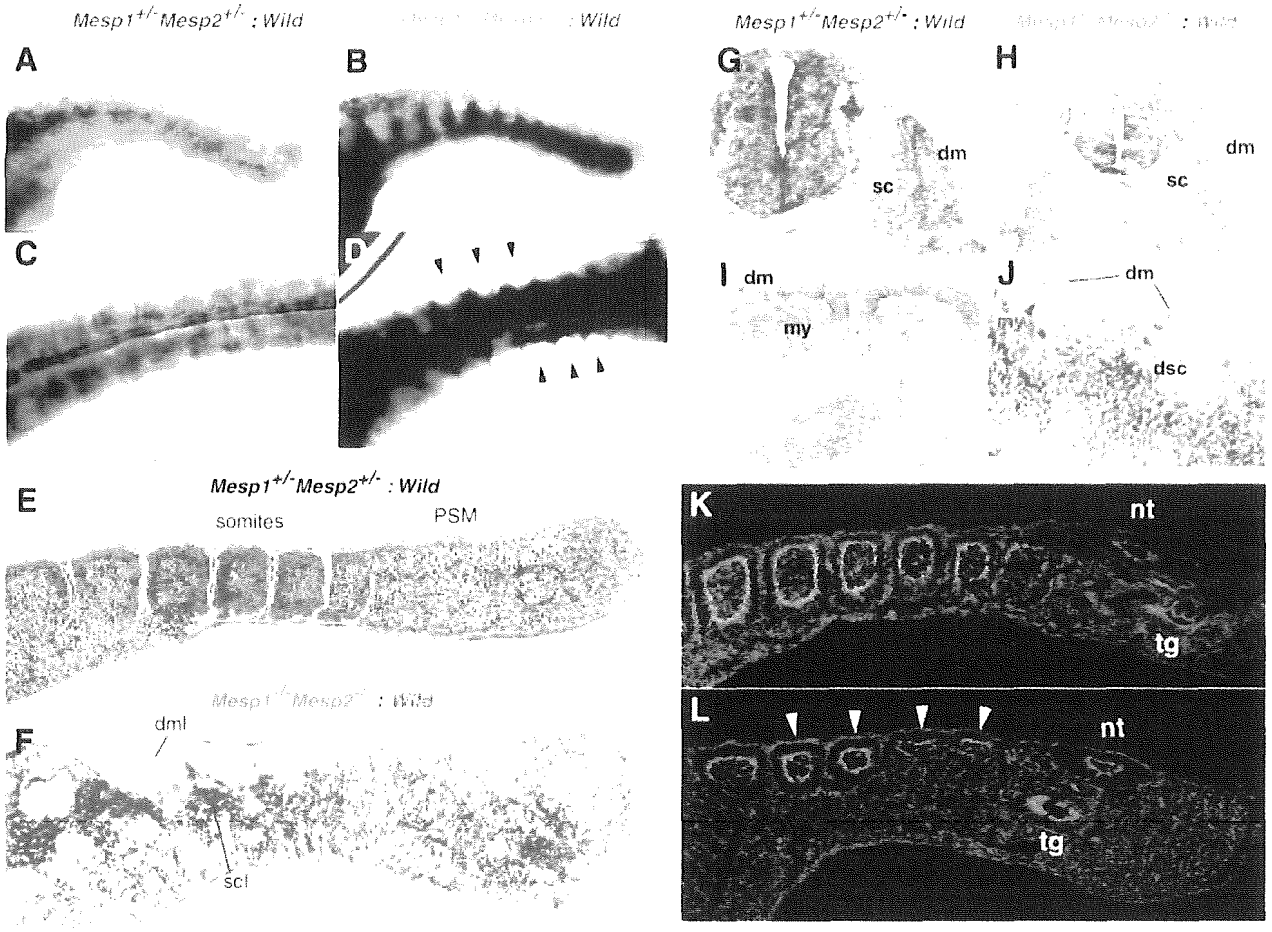

Fig. 5. Mesp1/Mesp2 double-null cells fail to contribute to epithelial somites or to the dermomyotome. (A-D) Tail regions from X-gal-stained whole-mount specimens of control (A,C) and double-null (B,D) chimeric embryos. (A,B) Lateral view. (C,D) Dorsal view. The blue double-heterozygous cells are randomly distributed in the control embryo, whereas the Mesp1/Mesp2 double-null cells are excluded from the lateral region of the somites (arrowheads in D). (E,F) Parasagittal sections of tails from chimeric embryos. (E) The labeled cells are randomly located in the control chimera. (F) The two types of cells are randomly mixed in the PSM, whereas the dermomyotome-like epithelium consisted exclusively of wild-type cells and the sclerotome-like compartment contained mostly Mesp1/Mesp2 double-null cells. Note that normal epithelial somites are not formed in this chimera. (G,H) Transverse sections show elimination of Mesp1/Mesp2 double-null cells from the dermomyotome. (I,J) The dermomyotome-like epithelium in the Mesp1/Mesp2 double-null chimeric embryo gives rise to dermomyotome, myotome (arrowhead in J) and the dorsal part of the sclerotome. Red arches indicate the inner surface of dermomyotome. (K,L) AlexaFluor 488-labeled phalloidin staining shows normal epithelialization of somites in the control chimera (K) and restriction of epithelialization in the dermomyotome-like compartment in the Mesp1/Mesp2 double-null chimera (L). dm, dermomyotome; dml, dermomyotome-like epithelium; dsc, dorsal part of the sclerotome; my, myotome; nt, neural tube; sc, sclerotome; scl, sclerotome-like compartment; tg, tail gut.

the anterior PSM. This is because 50% of cells cannot undergo suppression of Dll1 even in the future rostral half region. Therefore, our finding of a normal rostro-caudal pattern in the dermomyotome of double-null chimeras is surprising and raises the question of whether wild-type cells can be normally patterned in the presence of surrounding Mesp1/Mesp2 double-null cells. To determine how the rostro-caudal pattern in the dermomyotome is formed in the PSM, we examined the expression pattern of *Dll1* (Bettenhausen et al., 1995), the stripe expression profile of which is established in the anteriormost PSM via the function of Mesp2 (Takahashi et al., 2000). The *lacZ*-expressing Mesp1/Mesp2 double-null cells were subsequently found to be consistently localized in the sclerotome-like region, where *Dll1* expression was abnormally expanded (Fig. 6C,D). In the dermomyotome-like region, however, *Dll1* expression in the caudal half was normal. Intriguingly, strong *Dll1* expression in the anteriormost PSM was suppressed in a rostrally adjoining cell population, which is mainly occupied by wild-type cells (Fig. 6C,D, arrows). This implies that wild-type cells and Mesp1/Mesp2 double-null cells rapidly segregate at S-1 to S0, after which the rostro-caudal pattern of *Dll1* expression is formed in the partially segregated wild-type cell population but not in the randomly mixed cell population. In other words, the separation from Mesp1/Mesp2 double-null cells enabled normal rostro-caudal patterning of wild-type cells.

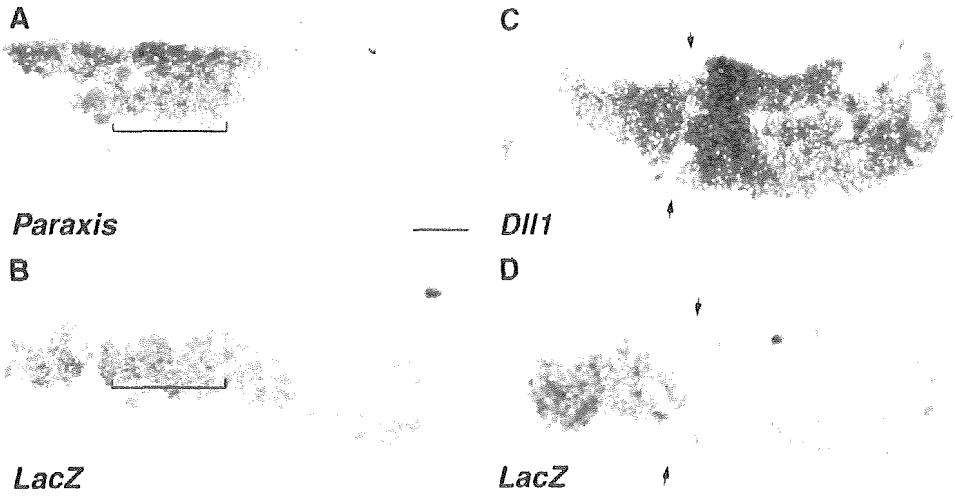

Fig. 6. (A,B) Mesp1/Mesp2 double-null cells express *Paraxis*. Adjacent parasagittal sections of the Mesp1/Mesp2 double-null chimeric embryo were stained for either *Paraxis* (A) or *lacZ* (B). Note that the expression domains of the two genes overlap in the medial sclerotomal region (brackets). (C,D) The rostro-caudal pattern in the dermomyotome is formed in a partially segregating wild-type cell population. Adjacent sections of the Mesp1/Mesp2 double-null chimeric embryos were stained for *Dll1* (C) or *lacZ* (D) mRNA. Red outlines demarcate the dorsal dermomyotome-like compartments. Note that suppression of *Dll1* expression occurs in a region mostly occupied by wild-type cells (arrows). Scale bar: 100 μm.

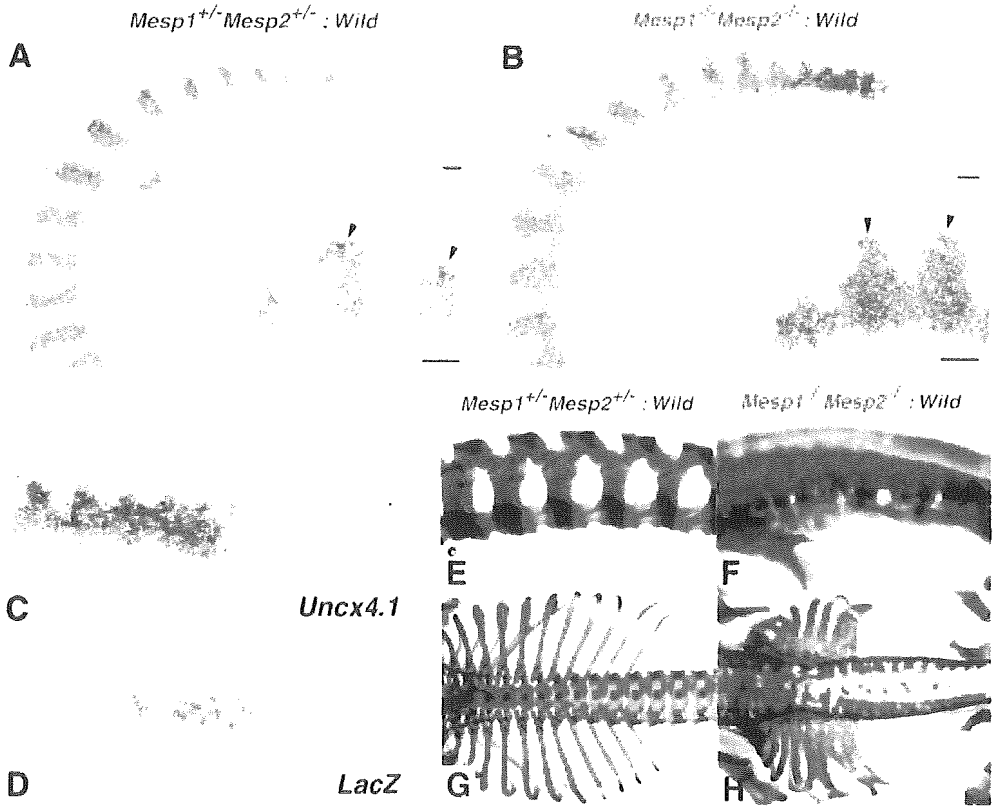

Fig. 7. Rostro-caudal patterning of the sclerotome is disrupted in Mesp1/Mesp2 double-null chimeric embryos. (A) The control chimeric embryos exhibit normal stripe patterns of *Uncx4.1* expression throughout the somite region. (B) The Mesp1/Mesp2 double-null chimeric embryos exhibit continuous *Uncx4.1* expression in the ventral sclerotomal region. Note that caudal localization of *Uncx4.1* expression is normal in the dermomyotome and dorsal sclerotome. The insets show a higher magnification of lumbar somites. (C,D) Adjacent sections showing that *lacZ*-expressing Mesp1/Mesp2 double-null cells express *Uncx4.1*. (E-H) The Mesp1/Mesp2 double-null chimeric fetus exhibits caudalization of the vertebrae and of the proximal ribs. (E) The control chimeric fetus shows normal metameric arrangement of the neural arches. (F) The Mesp1/Mesp2 double-null chimeric fetus shows severe fusion of the pedicles and the laminae of neural arches. (G) The control chimeric fetus has normal arrangement of ribs. (H) The double-null chimeric fetus shows severe fusion of the proximal elements of the ribs. Scale bars: 100 μm.

Mesp2-null fetuses display caudalized vertebrae with extensive fusion of the pedicles of neural arches and proximal elements of the ribs (Saga et al., 1997). The Mesp1/Mesp2 double-null chimeric fetuses also exhibited fusion of the pedicles of neural arches and the proximal ribs (Fig. 7E-H). Furthermore, the vertebrae of severe chimeric fetuses were indistinguishable from those of Mesp2-null fetuses. These observations indicate that Mesp1/Mesp2 double-null cells can differentiate into caudal sclerotome and possibly contribute to chondrogenesis.

Discussion

Mesp1 and Mesp2 not only exhibit similar expression patterns but also share common bHLH domains as transcription factors. Previous studies using gene replacement experiments (Saga, 1998) (Y.S. and S.K., unpublished) indicate that these genes can compensate for each other. However, the early lethality of double knockout mice hampered any further detailed analysis of somitogenesis. An obvious strategy to further elucidate the functions of Mesp1 and Mesp2 was, therefore, the generation of a conditional knockout allele for *Mesp2* in *Mesp1* disrupted cells in which the Cre gene is specifically activated in the paraxial mesoderm, which is now underway. Chimera analysis is also a powerful method as an alternative strategy. Comparisons of chimeras, composed of either Mesp2-null or Mesp1/Mesp2 double-null cells, made it possible to determine the contribution of Mesp1 to somitogenesis. Our results indicate that Mesp1 has redundant functions in the epithelialization of somitic mesoderm and additionally, by chimeric analysis, we were able to demonstrate the cell autonomy of Mesp1 and Mesp2 function during some critical steps of somitogenesis.

The relative contributions of Mesp1 and Mesp2 to somitogenesis

In Mesp1-null mice, epithelial somites with normal rostro-caudal polarity are generated, whereas Mesp2-null mice exhibit defects in both the generation of epithelial somites and the establishment of rostro-caudal polarity. Thus, it seems likely that Mesp2 function is both necessary and sufficient for somitogenesis. However, dermomyotome formation was observed, without normal segmentation, even in Mesp2-null mice. In view of the apparent redundant functions of Mesp1 and Mesp2 in somitogenesis, as demonstrated by our previous gene replacement study, it was possible that the Mesp1/Mesp2 double-null embryo would exhibit a much more severe phenotype in relation to somitogenesis. In our chimera analyses, both Mesp2-null and Mesp1/Mesp2 double-null cells exhibited complete caudalization of somitic mesoderm, indicating that Mesp1 function is not sufficient to rescue Mesp2 deficiency and restore rostro-caudal polarity. Likewise, both Mesp2-null and Mesp1/Mesp2 double-null cells were incapable of forming an initial segment boundary, showing that the contribution of Mesp1 is also minor during this process. By contrast, whereas Mesp1/Mesp2 double-null cells lacked any ability to epithelialize, Mesp2-null cells were occasionally integrated into epithelial somites and dermomyotome, indicating that the contribution of Mesp1 to epithelialization is significant and that Mesp1 can function in the absence of Mesp2 (Fig. 8). We therefore postulate that the epithelialization of dermomyotome, observed in Mesp2-null embryos, is dependent on Mesp1.

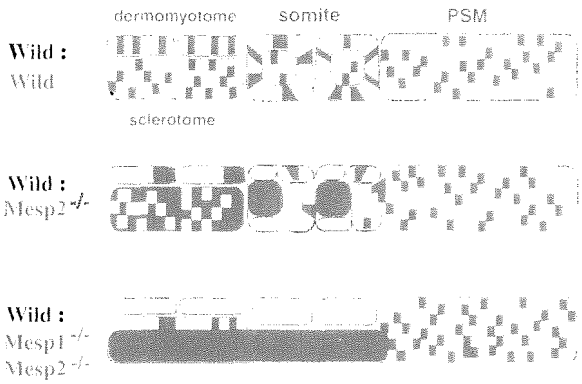

Fig. 8. A schematic summarization of the Mesp1/Mesp2 chimera experiments. Mesp1/Mesp2 double-null cells can contribute to neither epithelial somite nor dermomyotome formation, whereas Mesp2-null cells can partially contribute to both somites and dermomyotome. Red outlines indicate epithelialized tissues (epithelial somites, dermomyotomes and abnormal small clusters).

Mesp factors are cell autonomously required for epithelialization of somitic mesoderm but may also be non-cell autonomously required for morphological boundary formation

Conventional interpretations of the results of chimera analysis are generally based upon the regulative development of the vertebrate embryo and argue cell autonomy of specific gene functions in embryogenesis (Ciruna et al., 1997; Brown et al., 1999; Kitajima et al., 2000; Koizumi et al., 2001). Mesp1/Mesp2 double-null cells failed to form epithelial somites, even in the presence of surrounding wild-type cells. In addition, they were incapable of contributing to dermomyotome, where cell sorting occurs. This strongly suggests that Mesp factors are cell autonomously required for the epithelialization of somitic mesoderm. However, we also found striking non-cell autonomous effects of Mesp mutant cells on wild-type cell behaviors. That is, both types of Mesp mutant cell not only failed to undergo normal somitogenesis, but also inhibited the normal morphogenesis of wild-type cells. This implies that there are non-cell autonomous roles for Mesp factors in the establishment of the future somite boundary, as we will discuss further.

Initial epithelial somite formation is achieved by the mesenchymal-epithelial transition of cells located in the anterior PSM. A future somite boundary is established at a specific position in the PSM, followed by gap formation between the mesenchymal cell populations. Subsequently, cells located anterior to the boundary are epithelialized. This process is known to be mediated by an inductive signal from cells posterior to the boundary (Sato et al., 2002). Therefore, defects in epithelial somite formation can be explained in two principal ways: a lack of cellular ability to epithelialize (cell autonomous) and a lack of an inducing signal, which is produced in the anterior PSM by a mechanism mediated by Notch signaling (thus non-cell autonomous). In the case of chimeras of Mesp1/Mesp2 double-null cells, no local

boundary formed by locally distributed wild-type cells was observed, i.e. even a gap between wild-type cells was never observed in the mixture of Mesp1/Mesp2 double-null cells and wild-type cells. It is likely, therefore, that the wild-type cell population can form a boundary only after separation from Mesp1/Mesp2 double-null cells (Fig. 8). By contrast, some local boundaries between epithelial wild-type cell clusters were occasionally observed in chimeras with Mesp2-null cells. Considering that there is functional redundancy between these transcription factors, it is possible that either Mesp1 or Mesp2 is necessary for the formation of a signaling center or source of the putative inductive signal. Hence, we cannot exclude the possibility that the lack of Mesp function may affect non-cell autonomous generation of the inductive signal in the anterior PSM.

Formation of epithelial somites requires paraxis, which is a transcription factor (Burgess et al., 1996; Nakaya et al., 2004). We observed that Mesp1/Mesp2 double-null cells at the medial sclerotomal region expressed *Paraxis*, indicating that Mesp factors are not absolutely required for *Paraxis* expression. Defects in epithelial somite formation in paraxis-null embryos, with normal *Mesp2* expression (Johnson et al., 2001), and in Mesp2-null embryos, with normal *Paraxis* expression, imply that epithelial somite formation independently requires both gene functions.

Mesp2 is cell autonomously required for the acquisition of rostral properties

The distribution of Mesp2-null cells in the Mesp2-null chimeric embryos may appear somewhat paradoxical, as they are localized at the rostral side in the incomplete somites but at the caudal side in the dermomyotome. Initial localization at the rostral and central region, however, is likely to be due to the relative lack of epithelialization functions. In mammalian and avian embryos, mesenchymal-to-epithelial conversion of the PSM commences from the rostral side of the future somite boundary, i.e. the caudal margin of the presumptive somite (Duband et al., 1987). Epithelialization then proceeds anteriorly in the dorsal and ventral faces and in such a process, Mesp2-null cells, which are less able to participate in epithelialization, may therefore be pushed to the central and rostral sides. Thus, the majority of the Mesp2-null cells localize to the central, prospective sclerotomal region and a small number of them are integrated in the future dermomyotomal region. The incomplete somites then undergo reorganization into dermomyotome and sclerotome, and small numbers of Mesp2-null cells in the dermomyotome may be sorted out to the caudal end. Therefore, the apparently complex distribution pattern of Mesp2-null cells is likely to reflect a combination of defects in epithelialization and rostro-caudal patterning. In the incomplete segments of Mesp2-null chimeric embryos, the Mesp2-null cells fail to acquire rostral properties even when localized at the rostral side. Moreover, in the dermomyotome, where rostro-caudal patterning is rescued, Mesp2-null cells are mostly localized in the caudal region. These observations suggested that the requirement of Mesp2 for the acquisition of rostral properties is cell autonomous. Similarly, it has been reported that presenilin 1 (Psen1) is required for acquisition of caudal half properties (Takahashi et al., 2000; Koizumi et al., 2001) and that Psen1-null cells cannot contribute to the caudal half of somites in chimeric embryos, showing cell autonomous roles for Psen1 (Koizumi et al., 2001).

Mesp mutant cells affect the rostro-caudal patterning of somites due to the lack of cellular interaction with wild-type cells

In a previous study, we have shown that the rostro-caudal patterning of somites is generated by complex cellular interactions involved in positive and negative feedback pathways of Dll1-Notch and Dll3-Notch signaling, and regulation by Mesp2 in the PSM (Takahashi et al., 2003). In chimeras with either Mesp2-null or Mesp1/Mesp2 double-null cells, the mutant cells were distributed evenly and did not show any sorting bias in a rostro-caudal direction in the PSM. Since both Mesp2-null and Mesp1/Mesp2 double-null cells have the ability to form caudal cells, it is likely that if wild-type cells could occupy the rostral part of future somite regions and have the ability to sort in the PSM, a normal rostro-caudal patterning would be generated. We did not observe this, however, and conclude that the presence of mutant cells lacking Mesp factors must have disrupted normal cellular interactions via Notch signaling. Thus these non-cell-autonomous effects of our mutant cells are strongly supportive of our previous contention that rostro-caudal pattering is generated by cellular interactions via Notch signaling.

We thank Mariko Ikumi, Seiko Shinzawa, Eriko Ikeno and Shinobu Watanabe for general technical assistance. This work was supported by Grants-in-Aid for Science Research on Priority Areas (B) and the Organized Research Combination System of the Ministry of Education, Culture, Sports, Science and Technology, Japan.

References

Bettenhausen, B., Hrabe de Angelis, M., Simon, D., Guénet, J.-L. and Gossler, A. (1995). Transient and restricted expression during mouse embryogenesis of Dll1, a murine gene closely related to *Drosophila* Delta. *Development* **121**, 2407-2418.

Borycki, A. G. and Emerson, C. P., Jr (2000). Multiple tissue interactions and signal transduction pathways control somite myogenesis. *Curr. Top. Dev. Biol.* **48**, 165-224.

Brown, D., Wagner, D., Li, X., Richardson, D. A. and Olson, E. N. (1999). Dual role of the basic helix-loop-helix transcription factor scleraxis in mesoderm formation and chondrogenesis during mouse embryogenesis. *Development* **126**, 4317-4329.

Burgess, R., Cserjesi, P., Ligon, K. L. and Olson, E. N. (1995). Paraxis: a basic helix-loop-helix protein expressed in paraxial mesoderm and developing somites. *Dev. Biol.* **168**, 296-306.

Burgess, R., Rawls, A., Brown, D., Bradley, A. and Olson, E. N. (1996). Requirement of the *paraxis* gene for somite formation and musculoskeletal patterning. *Nature* **384**, 570-573.

Ciruna, B. G., Schwartz, L., Harpal, K., Yamaguchi, T. P. and Rossant, J. (1997). Chimeric analysis of *fibroblast growth factor receptor-1 (Fgfr1)* function: a role for FGFR1 in morphogenetic movement through the primitive streak. *Development* **124**, 2829-2841.

Duband, J. L., Dufour, S., Hatta, K., Takeichi, M., Edelman, G. M. and Thiery, J. P. (1987). Adhesion molecules during somitogenesis in the avian embryo. *J. Cell Biol.* **104**, 1361-1374.

Fan, C. M. and Tessier Lavigne, M. (1994). Patterning of mammalian somites by surface ectoderm and notochord: Evidence for sclerotome induction by a hedgehog homolog. *Cell* **79**, 1175-1186.

Gossler, A. and Hrabe de Angelis, M. (1997). Somitogenesis. *Curr. Top. Dev. Biol.* **38**, 225-287.

Johnson, J., Rhee, J., Parsons, S. M., Brown, D., Olson, E. N. and Rawls, A. (2001). The anterior/posterior polarity of somites is disrupted in Paraxis-deficient mice. *Dev. Biol.* **229**, 176-187.

Kitajima, S., Takagi, A., Inoue, T. and Saga, Y. (2000). MesP1 and MesP2

are essential for the development of cardiac mesoderm. *Development* **127**, 3215-3226.

Koizumi, K., Nakajima, M., Yuasa, S., Saga, Y., Sakai, T., Kuriyama, T., Shirasawa, T. and Koseki, H. (2001). The role of presenilin 1 during somite segmentation. *Development* **128**, 1391-1402.

Mansouri, A., Yokota, Y., Wehr, R., Copeland, N. G., Jenkins, N. A. and Gruss, P. (1997). Paired-related murine homeobox gene expressed in the developing sclerotome, kidney, and nervous system. *Dev. Dyn.* **210**, 53-65.

Nakaya, Y., Kuroda, S., Katagiri, Y. T., Kaibuchi, K. and Takahashi, Y. (2004). Mesenchymal-epithelial transition during somitic segmentation is regulated by differential roles of Cdc42 and Rac1. *Dev. Cell* **7**, 425-438.

Neidhardt, L. M., Kispert, A. and Herrmann, B. G. (1997). A mouse gene of the paired-related homeobox class expressed in the caudal somite compartment and in the developing vertebral column, kidney and nervous system. *Dev. Genes Evol.* **207**, 330-339.

Nieto, M. A., Gilardi-Hebenstreit, P., Charnay, P. and Wilkinson, D. G. (1992). A receptor protein tyrosine kinase implicated in the segmental patterning of the hindbrain and mesoderm. *Development* **116**, 1137-1150.

Nomura-Kitabayashi, A., Takahashi, Y., Kitajima, S., Inoue, T., Takeda, H. and Saga, Y. (2002). Hypomorphic *Mesp* allele distinguishes establishment of rostro-caudal polarity and segment border formation in somitogenesis. *Development* **129**, 2473-2481.

Pourquié, O. (2001). Vertebrate somitogenesis. *Annu. Rev. Cell. Dev. Biol.* **17**, 311-350.

Saga, Y. (1998). Genetic rescue of segmentation defect in MesP2-deficient mice by MesP1 gene replacement. *Mech. Dev.* **75**, 53-66.

Saga, Y. and Takeda, H. (2001). The making of the somite: molecular events in vertebrate segmentation. *Nat. Rev. Genet.* **2**, 835-845.

Saga, Y., Hata, N., Kobayashi, S., Magnuson, T., Seldin, M. and Taketo, M. M. (1996). MesP1: A novel basic helix-loop-helix protein expressed in the nascent mesodermal cells during mouse gastrulation. *Development* **122**, 2769-2778.

Saga, Y., Hata, N., Koseki, H. and Taketo, M. M. (1997). *Mesp2*: a novel mouse gene expressed in the presegmented mesoderm and essential for segmentation initiation. *Genes Dev.* **11**, 1827-1839.

Saga, Y., Miyagawa-Tomita, S., Takagi, A., Kitajima S., Miyazaki, J. and Inoue, T (1999). MesP1 is expressed in the heart precursor cells and required for the formation of a single heart tube. *Development* **126**, 3437-3447.

Sato, Y., Yasuda, K. and Takahashi, Y. (2002). Morphological boundary forms by a novel inductive event mediated by Lunatic fringe and Notch during somitic segmentation. *Development* **129**, 3633-3644.

Takahashi, Y., Koizumi, K., Takagi, A., Kitajima, S., Inoue, T., Koseki, H. and Saga, Y. (2000). Mesp2 initiates somite segmentation through the Notch signalling pathway. *Nat. Genet.* **25**, 390-396.

Takahashi, Y., Inoue, T., Gossler, A. and Saga, Y. (2003). Feedback loops comprising Dll1, Dll3 and Mesp2, and differential involvement of Psen1 are essential for rostrocaudal patterning of somites. *Development* **130**, 4259-4268.

Zambrowicz, B. P., Imamoto, A., Fiering, S., Herzenberg, L. A., Kerr, W. G. and Soriano, P. (1997). Disruption of overlapping transcripts in the ROSA beta geo 26 gene trap strain leads to widespread expression of beta-galactosidase in mouse embryos and hematopoietic cells. *Proc. Natl. Acad. Sci. USA* **94**, 3789-3794.

J Toxicol Pathol 2005; 18: 41–46

Original

Electron Microscopical Evidence of the Protective Function of Thioredoxin (TRX/ADF) Transgene against 2,3,7,8-tetrachlorodibenzo-*p*-dioxin (TCDD)-induced Cellular Toxicity in the Liver and Brain

Byung-Il Yoon[1,5], Toyozo Kaneko[1], Yoko Hirabayashi[1], Takayoshi Imazawa[2], Akiyoshi Nishikawa[2], Yukio Kodama[1], Jun Kanno[1], Junji Yodoi[4], Jeong-Hee Han[5], Masao Hirose[2], and Tohru Inoue[3]

[1]Division of Cellular and Molecular Toxicology
[2]Department of Pathology
[3]Safety and Research Center of National Institute of Health Sciences, Tokyo 158–8501, Japan
[4]Department of Biological Responses, Institute for Virus Research, Kyoto University, Kyoto, Japan
[5]Department of Veterinary Medicine, Kangwon National University, Chunchcon 200–701, Korea

Abstract: The present study was performed to assess the protective role of thioredoxin/adult T-cell leukemia-derived factor (TRX/ADF) on the liver and brain cell damages induced by 2,3,7,8-tetrachlorodibenzo-*p*-dioxin (TCDD) in ADF wild-type (WT) and transgenic (Tg) mice. The ADF WT and Tg mice were intraperitoneally injected with a single dose of TCDD (150 μg/kg body weight). One day after the treatment, the liver and brain tissues were examined electron microscopically to evaluate the cellular toxicity. In the ADF WT mice, marked reduction of subcellular components, such as mitochondria, rough endoplasmic reticula, and glycogen granules, as well as swelling of the remaining mitochondria, were evident in the liver cells. However, attenuation of these changes was evident in TCDD-treated TRX/ADF mice. Similar subcellular changes noted in the neuronal cells of TCDD-treated WT mice were also attenuated in Tg mice. The results suggest that oxidative cellular damage contributes to the acute toxicity induced by TCDD and that TRX/ADF protects against it. (J Toxicol Pathol 2005; **18**: 41–46)

Key words: Ah receptor, brain, liver, 2,3,7,8-tetrachlrodibenzo-*p*-dioxin (TCDD), thioredoxin/adult T-cell leukemia-derived factor (TRX/ADF), transgenic (Tg) mouse

Introduction

As one of the aromatic hydrocarbons, 2,3,7,8-tetrachlorodibenzo-*p*-dioxin (TCDD) is a widely spread environmental pollutant that has a broad spectrum of toxic effects on a variety of tissues such as the thymus, liver, testes and central nervous system in mammals[1–6]. Although a number of studies have shown that the toxic effects of TCDD are mediated by intracytoplasmic aromatic hydrocarbon receptor (AhR)[7–9], the toxic mechanism of TCDD on the target organs is still not fully understood. Among the toxic events, oxidative stress is considered to play a major role in the toxic mechanism of TCDD, as characterized by marked increases of lipid peroxidation, the formation of reactive oxygen species, and DNA single-strand break[9–14].

Exogenous xenobiotics, such as aromatic hydrocarbons, result in profound induction of cytochrome P450 enzymes in the liver, resulting in the generation of reactive oxygen species[15,16]. On the other hand, the brain is rich in peroxidizable fatty acids and has relatively low catalase activity[17]. Therefore, these organs are considered to be highly susceptible to oxidative stresses[18]. In fact, the contribution of oxidative stress in TCDD-induced cellular damage of the liver and brain has been suggested in previous studies[13,18–22].

Adult T-cell leukemia-derived factor (ADF) is a human thioredoxin (TRX) associated with the reduction/oxidation (redox) regulation of the cellular environment[23]. TRX/ADF is a stress-inducible protein and its expression is up-regulated after viral infection as well as in cellular stress conditions induced by oxidative agents such as hydrogen peroxide or diamide, irradiation with X-rays and ultraviolet

Received: 24 September 2004, Accepted: 15 February 2005
Mailing address: Byung-Il Yoon, Department of Veterinary Medicine, College of Animal Resources Sciences, Kangwon National University, 192–1 Hyoja2-dong, Chunchcon, Kangwon 200–701, Republic of Korea
TEL: 82-33-250-8679 FAX: 82-33-244-2367
E-mail: byoon@kangwon.ac.kr

light, or ischemic reperfusion[23]. Previous studies have shown that TRX/ADF plays a role in the cellular defense mechanism against oxidative cellular damage via the regulation of intracellular redox status, since exogenously administered TRX/ADF protected cells from oxidative cellular injury[24,25].

We recently reported for the first time the protective function of TRX/ADF against TCDD-induced hematotoxicity in ADF transgenic (Tg) mice, indicating oxidative stress contributes to the hematotoxic mechanism of TCDD[26]. We hypothesized in the present study that overexpression of TRX/ADF might also be effective for protection against the toxic effects of TCDD on the liver and brain tissues in which oxidative stress has also been implicated in the toxic mechanism. For this purpose, we injected TCDD with a dosage capable of inducing oxidative stress in the liver following acute exposure[21], to ADF wild-type (WT) and transgenic (Tg) mice, and then compared subcellular changes electron microscopically in the liver and brain tissues.

Materials and Methods

Animals

TRX/ADF overexpressed mice (ADF Tg mice), originally produced by Dr. A. Mitsui[27], were maintained in a laboratory facility with a 12:12-hour light-dark cycle at an ambient temperature of 21 ± 2°C at the National Institute of Health Sciences (NIHS) of Japan by breeding ADF WT and Tg mice. Animals were screened by PCR of their tail DNA to determine their genotypes. At 8 weeks of age, male ADF WT and Tg mice (23.5–24.8 g) were transferred to a vinyl isolator established in a hazard room designed to prevent contamination from the outside environment and randomly allocated within the same genotype to housing with 6 animals per cage. A pelleted basal diet (CRF-1; Funabashi Farm, Funabashi, Japan) and tap water were provided *ad libitum* throughout the study.

Chemical

TCDD was obtained from Radian International, Cambridge Isotope Laboratories, Inc. (Andover, MA, USA; purity: 98 %). TCDD was initially dissolved in a small volume of acetone and subsequently adjusted to the concentration of 10 μg/ml in olive oil.

Experimental design

ADF WT and Tg mice were divided into vehicle controls and TCDD treatment groups, each consisting of 6 animals. After one week of acclimation, TCDD at 150 μg/kg was intraperitoneally injected once to animals of treatment groups, and the corresponding volume of olive oil was similarly injected to vehicle controls. The dosage of TCDD was selected based on previous study results that showed oxidative stress in the liver was induced by a single bolus injection to mice[21]. One day after the treatment, the animals were sacrificed by decapitation and then examined grossly. The liver and brain were then excised and their weights were measured.

The animal protocol was reviewed and approved by the Animal Care and Use Committee of the NIHS, Japan.

Morphological assessment

For histological examination, liver tissues in all animals were fixed in 10% neutral buffered formalin (pH 7.4). After routine processing, the paraffin-embedded sections were stained with hematoxylin and eosin and then examined histopathologically under a light microscope.

For electron microscopical examination, tissue specimens from the liver and cerebral cortex were respectively prepared from three animals each of the control and treatment groups of ADF WT and Tg mice. Small tissue blocks, sized 1 mm^3, were fixed with 2.5% glutaraldehyde in 0.2 M Sorenson's sodium phosphate buffer, pH 7.2, for 8 hours at 4°C. After washing with 0.1 M PBS (pH 7.4), the tissues were post-fixed with 1% osmium tetroxide for 90 minutes. After washing in 0.1 M PBS, the tissues were dehydrated with ethanol and propylene oxide and then embedded in Epon 812. Ultrathin sections were double-stained with uranyl acetate and lead citrate. The sections were examined with JEOL-1200 EX II electron microscope (JEOL, Tokyo, Japan).

Results

After one day of TCDD treatment, absolute liver weight had decreased to 71.4% of the vehicle control group in ADF WT mice and 83.2% in ADF Tg mice (data not shown).

Histologically, apoptotic liver cell debris and also focal liver cell necrosis were sparsely observed in the centrilobular areas of both TCDD-treated WT and ADF Tg mice, without showing apparent difference in the severity between genotypes (data not shown). Vehicle control animals did not show such liver cell changes in either genotype.

Electron microscopically, liver cells of the WT mice treated with TCDD exhibited a prominent decrease of cytoplasmic glycogen granules and rough endoplasmic reticula (RERs) and an increase of smooth endoplasmic reticula (SERs) (Fig. 1B). The number of mitochondria was also decreased and the remaining mitochondria showed swelling with disorganized cristae and lucent matrix. Increased fat droplets were also evident in the cytoplasm of less affected hepatocytes. On the other hand, transgene of Trx/ADF notably attenuated these morphological changes following TCDD treatment (Fig. 1C). In the cerebral cortex, neuronal cells showed a decrease in the number of RERs, ribosomes and mitochondria in WT mice treated with TCDD (Fig. 2B) but not in ADF Tg mice treated similarly with TCDD (Fig. 2C). Vehicle control animals did not show such neuronal cell changes in either genotype.

Discussion

In the present study, acute treatment with TCDD

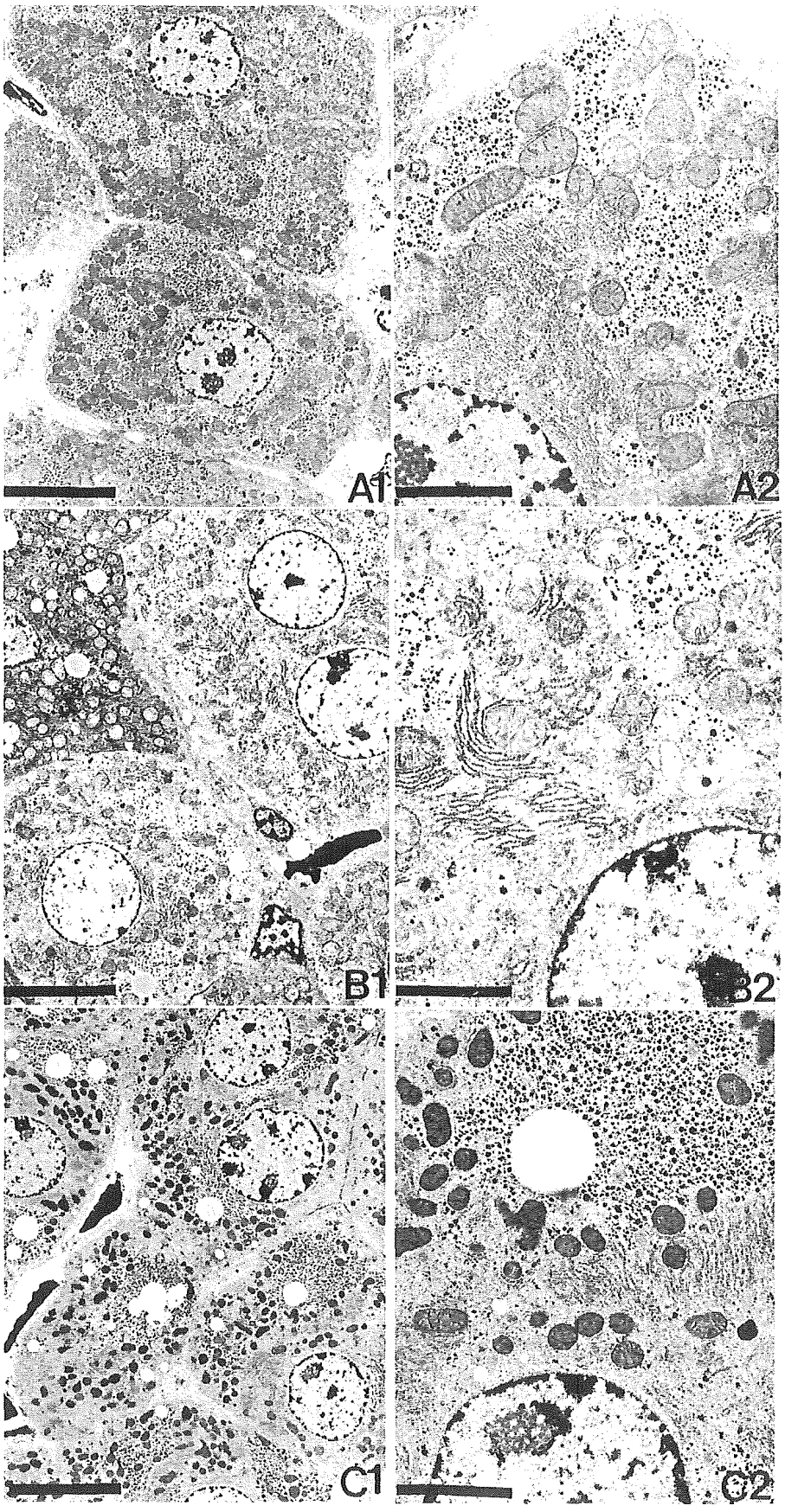

Fig. 1. Electron micrographs of liver cells from ADF WT and Tg mice treated with vehicle or TCDD. (A) Vehicle-treated ADF WT mouse, (B) TCDD-treated ADF WT mouse, and (C) TCDD-treated ADF Tg mouse. Note cytoplasmic swelling associated with a profound decrease of glycogen granules, RERs and mitochondria in the liver cells of the TCDD-treated ADF WT mouse (B). Swelling of the remaining mitochondria with disorganized cristae and lucent matrix is also evident (B). Attenuation of these morphological changes is evident in the TCDD-treated ADF Tg mouse (C). Uranyl acetate and lead citrate. Bar=10 μm (A1, B1, C1), Bar=3 μm (A2, B2, C2).

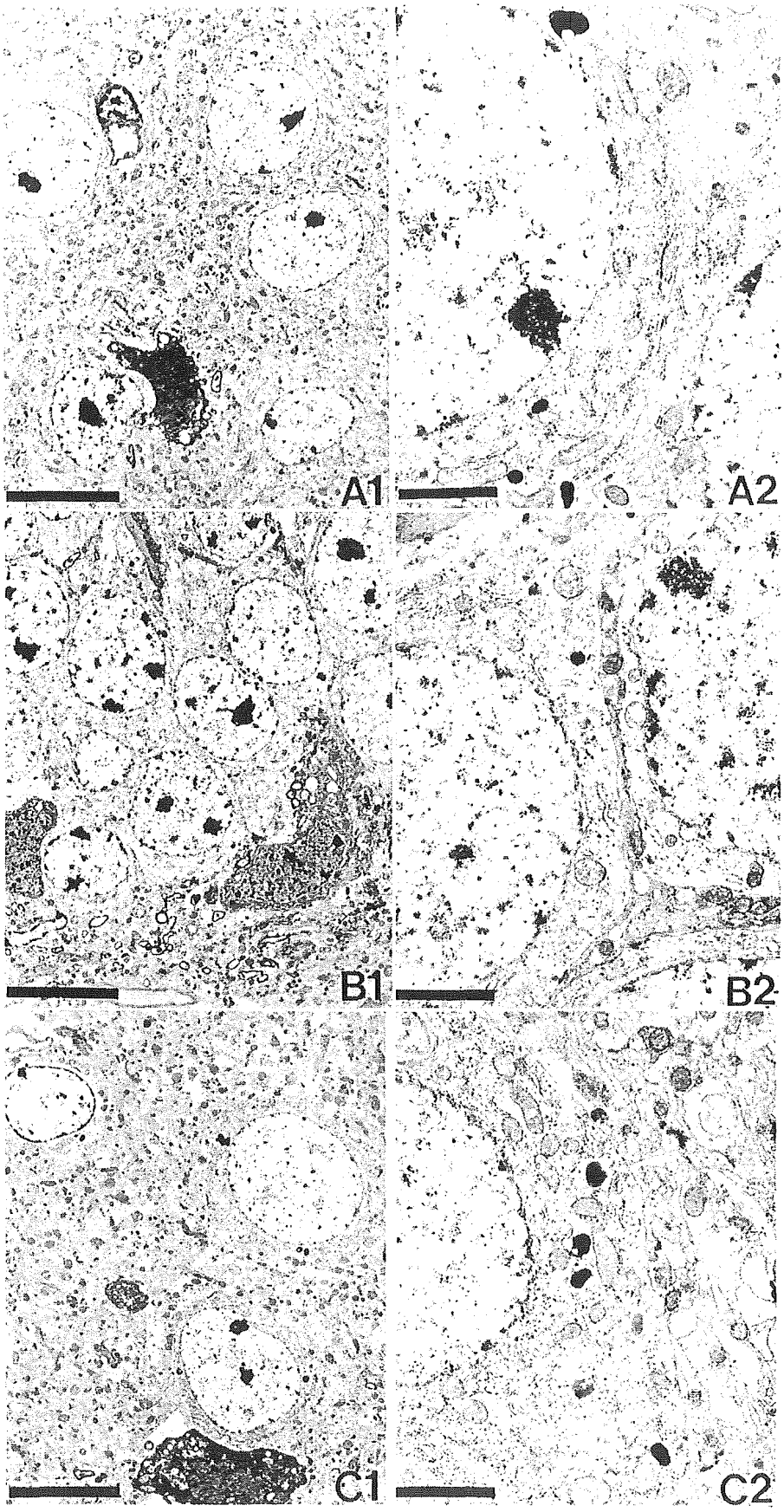

Fig. 2. Electron micrographs of neuronal cells in the cerebral cortex from ADF WT and Tg mice treated with vehicle or TCDD. (A) Vehicle-treated ADF WT mouse, (B) TCDD-treated ADF WT mouse, and (C) TCDD-treated ADF Tg mouse. Note the decrease of RER, ribosome and mitochondria in the cytoplasm of neuronal cells of the TCDD-treated ADF WT mouse (B). In the TCDD-treated ADF Tg mouse, mitochondrial swelling is also evident, but attenuation of the morphological changes can be seen, too. (C). Uranyl acetate and lead citrate. Bar=10 μm (A1, B1, C1), Bar=2 μm (A2, B2, C2).

induced ultrastructural alterations in the cytoplasmic components of liver cells characterized by prominent decrease of glycogen granules and RERs, proliferation of SERs, decrease and degradation of mitochondria, and increase of lipid droplets. These subcellular alterations were mostly consistent with those noted in the guinea pig liver following TCDD treatment[28], but concentric membrane arrays in the liver cells were not evident in the present study, presumably due to the different experimental protocol or the different species used in the studies. In the cerebral neuronal cells in the present study, alterations in subcellular components by TCDD were also evident, despite the changes being less profound than those in the liver cells. These subcellular changes in the liver and neuronal cells may represent the cytotoxic outcome of TCDD due to oxidative cellular damage and also cellular adaptation including detoxification.

Effective prevention of TCDD-induced toxicity by administration of antioxidants such as oltipraz[5-(2-pyrazinyl)-4-methyl-1,2-dithiol-3-thione] or butylated hydroxyanisole, or by pretreatment with vitamins A and E further supports the hypothesis that oxidative processes are involved in TCDD-induced toxicity[29,30]. Attenuation of subcellular changes in the liver and neuronal cells by transgene of TRX/ADF in the present study indicates the critical role of oxidative stress in the toxic events induced by TCDD, and also the protective function of ADF/TRX in these organs, as in our previous study of TCDD-induced bone marrow toxicity[26]. The protective effect of TRX/ADF against oxidative cellular damage is believed to be achieved by free radical scavengers[31], activation of DNA repair enzymes, such as activator protein endonuclease (Ref-1; redox factor-1)[32], and activation of nuclear factor-kappa B (NF-kB)[33].

Taken together, the results of our present study strongly suggest that the acute toxic effect induced in the liver and brain by a single large dose of TCDD is due to oxidative cellular damage, and that TRX/ADF plays a role in protection against TCDD-induced acute toxicity. Considering the routes and concentrations of TCDD exposed to humans, research on the effect of extremely low doses of TCDD by oral ingestion on the oxidative cellular damage of target organs is clearly warranted.

References

1. Kociba RJ, Keeler PA, Park CN, and Gehring PJ. 2,3,7,8-Tetrachlorodibenzo-*p*-dioxin (TCDD): results of a 13-week oral toxicity study in rats. Toxicol Appl Pharmacol. **35**: 553–574. 1976.
2. Chahoud I, Krowke R, Schimmel A, Merker HJ, and Neubert D. Reproductive toxicity and pharmacokinetics of 2,3,7,8-tetrachlorodibenzo-*p*-dioxin. 1. Effects of high doses on the fertility of male rats. Arch Toxicol. **63**: 432–439. 1989.
3. Funseth E and Ilbäck N-G. Effects of 2,3,7,8-tetrachlorodibenzo-*p*-dioxin on blood and spleen natural killer (NK) cell activity in the mouse. Toxicol Lett. **60**: 247–256. 1992.
4. Ivens IA, Loser E, Rinke M, Schmidt U, and Neupert M. Toxicity of 2,3,7,8-tetrachlorodibenzo-*p*-dioxin in rats after single oral administration. Toxicology. **73**: 53–69. 1992.
5. Ivens IA, Loser E, Rinke M, Schmidt U, and Mohr U. Sunchronic toxicity of 2,3,7,8-tetrachlorodibenzo-*p*-dioxin in rats. Toxicology. **83**: 181–201. 1993.
6. Erin Staples E, Murante FG, Fiore NC, Gasiewicz TA, and Silverstone AE. Thymic alteration induced by 2,3,7,8-tetrachlorodibenzo-*p*-dioxin are strictly dependent on aryl hydrocarbon receptor activation in hemopoietic cells. J Immunol. **160**: 3844–3854. 1998.
7. Poland A and Knutson JC. 2,3,7,8-Tetrachlorodibenzo-*p*-dioxin and related halogenated aromatic hydrocarbons: examination of the mechanism of toxicity. Annu Rev Pharmacol Toxicol. **22**: 517–554. 1982.
8. Cook JC, Gaido KW, and Greenlee WF. Ah receptor: relevance of mechanistic studies to human risk assessment. Environ Health Perspect. **76**: 71–77. 1987.
9. Alsarif NZ, Lawson T, and Stohs SJ. Oxidative stress induced by 2,3,7,8-tetrachlorodibenzo-*p*-dioxin is mediated by the aryl hydrocarbon (Ah) receptor complex. Toxicology. **92**: 39–51. 1994a.
10. Stohs SJ, Hassan MQ, and Murray WJ. Lipid peroxidation as a possible cause of TCDD toxicity. Biochem Biophys Res Commun. **111**: 854–859. 1983.
11. Mohammadpour H, Murray WJ, and Stohs SJ. 2,3,7,8-Tetrachlorodibenzo-*p*-dioxin -induced lipid peroxidation in genetically responsive and non-responsive mice. Arch Environ Contam Toxicol. **17**: 645–650. 1988.
12. Wahba ZZ, Lawson TA, Murray WJ, and Stohs SJ. Factors influencing the induction of DNA single strand breaks in rats by 2,3,7,8-tetrachlorodibenzo-*p*-dioxin (TCDD). Toxicology. **58**: 57–69. 1989.
13. Al-Bayati ZAF, Murray WJ, and Stohs SJ. 2,3,7,8-Tetrachlorodibenzo-*p*-dioxin-induced lipid peroxidation in hepatic and extrahepatic tissues of male and female rats. Arch Environ Contam Toxicol. **16**: 159–166. 1987.
14. Alsharif NZ, Schlueter WJ, and Stohs SJ. Stimulation of NADPH-dependent reactive oxygen species formation and DNA damage by 2,3,7,8-tetrachlorodibenzo-*p*-dioxin in rat peritoneal lavage cells. Arch Environ Contam Toxicol. **26**: 392–397. 1994b.
15. Stohs SJ. Oxidative stress induced by 2,3,7,8-tetrachlorodibenzo-*p*-dioxin (TCDD). Free Radic Biol Med. **9**: 79–90. 1990.
16. Bondy SC and Naderi S. Contribution of hepatic cytochrome P450 systems to the generation of reactive oxygen species. Biochem Pharmacol. **48**: 155–159. 1994.
17. Floyd RA. Antioxidants, oxidative stress, and degenerative neurological disorders. Proc Soc Exp Biol Med. **222**: 236–245. 1999.
18. Hassoun EA, Li F, Abushaban A, and Stohs SJ. Production of superoxide anion, lipid oxidation and DNA damage in the hepatic and brain tissues of rats after subchronic exposure to mixtures of TCDD and its congeners. J Appl Toxicol. **21**: 211–219. 2001.
19. Tritscher AM, Seacat AM, Yager JD, Groopman JD, Miller BD, Bell D, Sutter TR, and Lucier GW. Increased oxidative DNA damage in livers of 2,3,7,8-tetrachlorodibenzo-*p*-dioxin treated intact but not ovarectomized rats. Cancer Lett.

98: 219–225. 1996.
20. Hassoun EA, Wilt SC, Devito MJ, Van Birgelen A, Alsharif NZ, Birnbaum LS, and Stohs SJ. Induction of oxidative stress in brain tissues of mice after subchronic exposure to 2,3,7,8-tetrachlorodibenzo-*p*-dioxin. Toxicol Sci. **42**: 23–27. 1998.
21. Slezak BP, Hatch GE, DeVito MJ, Diliberto JJ, Slade R, Crisman K, Hassoun E, and Birnbaum LS. Oxidative stress in female B6C3F1 mice following acute and subchronic exposure to 2,3,7,8-tetrachlorodibenzo-*p*-dioxin (TCDD). Toxicol Sci. **54**: 390–398. 2000.
22. Senft AP, Dalton TP, Nebert DW, Genter MB, Hutchinson RJ, and Shertzer HG. Dioxin increases reactive oxygen production in mouse liver mitochondria. Toxicol Appl Pharmacol. **178**: 15–21. 2002.
23. Nakamura H, Nakamura K, and Yodoi J. Redox regulation of cellular activation. Annu Rev Immunol. **15**: 351–369. 1997.
24. Nakamura H, Matsuda M, Furuke K, Kitaoka Y, Iwata S, Toda K, Inamoto T, Yamaoka Y, Ozawa K, and Yodoi J. Adult T cell leukemia-derived factor/human thioredoxin protects endothelial F-2 cell injury caused by activated neutrophils or hydrogen peroxide. Immunol Lett. **42**: 75–80. 1994.
25. Yokomise H, Fukuse T, Hirata T, Ohkubo K, Go T, Muro K, Yagi K, Inui K, Hitomi S, and Mitsui A. Effect of recombinant human adult T cell leukemia-derived factor on rat lung reperfusion injury. Respiration. **61**: 99–104. 1994.
26. Yoon BI, Hirabayashi Y, Kaneko T, Kodama Y, Kanno J, Yodoi J, Kim DY, and Inoue T. Transgene expression of thioredoxin (Trx/ADF) protects against 2,3,7,8-tetrachlorodibenzo-*p*-dioxin (TCDD)-induced hematotoxicity. Arch Environ Contam Toxicol. **41**: 232–236. 2001.
27. Takagi Y, Mitsui A, Nishiyama A, Nozaki K, Sono H, Gon Y, Hashimoto N, and Yodoi J. Overexpression of thioredoxin in transgenic mice attenuates focal ischemic brain damage. Proc Natl Acad Sci USA. **96**: 4131–4136. 1999.
28. Turner JN and Collins DN. Liver morphology in guinea pigs administered either pyrolysis products of a polychlorinated biphenyl transformer fluid or 2,3,7,8-tetrachlorodibenzo-*p*-dioxin. Toxicol Appl Pharmacol. **67**: 417–429. 1983.
29. Hassan MQ, Stohs SJ, and Murray WJ. Inhibition of TCDD-induced lipid peroxidation, glutathione peroxidase activity and toxicity by BHA and glutathione. Bull Environ Contam Toxicol. **34**: 787–796. 1985.
30. Hassan MQ, Stohs SJ, and Murray WJ. Effects of vitamin E and A on TCDD-induced lipid peroxidation and other biochemical changes. Arch Environ Contam Toxicol. **14**: 437–442. 1985.
31. Tanaka T, Nishiyama Y, Okada K, Hirota K, Matsui M, Yodoi J, Hiai H, and Toyokuni S. Induction and nuclear translocation of thioredoxin by oxidative damage in the mouse kidney: independence of tubular necrosis and sulfhydryl depletion. Lab Invest. **77**: 145–155. 1997.
32. Walker LJ, Robson CN, Black E, Gillespie D, and Hickson ID. Identification of residues in the human DNA repair enzyme HAP1 (Ref-1) that are essential for redox regulation of Jun DNA binding. Mol Cell Biol. **13**: 5370–5376. 1993.
33. Schenk H, Klein M, Erdbrügger W, Dröge W, and Schulze-Osthoff K. Distinct effects of thioredoxin and antioxidants on the activation of transcription factor NF-kB and AP-1. Proc Natl Acad Sci USA. **91**: 1672–1676. 1994.

Toxicologic Pathology, 32(Suppl. 2):12–16, 2004

ISSN: 0192-6233 print / 1533-1601 online
DOI: 10.1080/01926230490451725

Mechanism of Benzene-Induced Hematotoxicity and Leukemogenicity: Current Review with Implication of Microarray Analyses

YOKO HIRABAYASHI,[1] BYUNG-IL YOON,[1,2] GUANG-XUN LI,[1] JUN KANNO,[1] AND TOHRU INOUE[3]

[1]*Division of Cellular and Molecular Toxicology, National Institute of Health Sciences, Tokyo 158-8501, Japan*
[2]*Department of Veterinary Medicine, Kangwon National University, Kangwon 200-701, Republic of Korea, Seoul National University, Seoul 151-742, Republic of Korea, and*
[3]*Biological Safety and Research Center, National Institute of Health Sciences, Tokyo 158-8501, Japan*

ABSTRACT

Benzene is a potent human leukemogen but the mechanism underlying benzene-induced leukemia remains an enigma due to a number of questions regarding the requirement of extraordinarily long exposure, a relatively low incidence of leukemia for genotoxicity of metabolites and a narrow dose range for leukemogenicity over marrow aplasia (overdoses tend to result in marrow aplasia). Moreover, there were previous controversies as to whether the cell cycle is upregulated or suppressed by the benzene exposure. Subsequently, it was found that the cell cycle is suppressed, but how leukemia develops under such suppression of hemopoiesis remains to be clarified. These questions were fortunately resolved with much effort. Benzene exposure was found to induce the expression of p21, an interlocking counterdevice for cell cycle: due to *p53* upregulation, thereby inducing the immediate suppression of the kinetics of hemopoietic progenitors followed by the prominent suppression of hemopoiesis. Intermittent benzene exposure (i.e., cessation of exposure during weekends, for example) allowed an immediate recovery from marrow suppression after terminating exposure, which induced continuous oscillatory changes in marrow hemopoiesis. Benzene-induced leukemia was chiefly due to such an oscillatory change in hemopoiesis, which epigenetically developed leukemia more than 1 year later. The mechanisms of benzene-induced leukemogenicity seem to differ between wild-type mice and mice lacking *p53*. For *p53* knockout mice, DNA damage such as weak mutagenicity or chromosomal damage was retained, and such damage induced consequent activation of proto-oncogenes and related genes, which led cells to undergo further neoplastic changes. In contrast, for wild-type mice carrying the *p53* gene, a marked oscillatory change in the cell cycle of the stem cell compartment seems to be important. Compatible and discriminative gene expression profiling between the *p53* knockout mice and wild-type mice was observed after benzene exposure by microarray analyses.

Keywords. Benzene; hematotoxicity; leukemogenicity; gene chip array; BUUV method; *p53*-KO; AhR-KO; hemopoietic progenitor cells.

INTRODUCTION

The mechanism of benzene-induced leukemia had long been an enigma until recently, when the unique cell kinetics of stem/progenitor cells during benzene exposure was elucidated. Leukemia induction by benzene inhalation was first reported in 1897, when Le Noire described multiple cases of leukemia among Parisian cobblers (Le Noir and Claude, 1897). However, the experimental induction of leukemia by benzene exposure was first reported about 20 years ago by Snyder et al. (1980) and our group (Cronkite et al., 1984, 1989). Recently, we demonstrated marked oscillatory changes in peripheral blood and bone marrow (BM)[1] cellularities during and following benzene inhalation, preceding the development of leukemia by about 1 year (Hirabayashi et al., 1998; Kawasaki et al., 2001; Yoon et al., 2001).

Address correspondence to: Tohru Inoue, Center for Biological Safety and Research, National Institute of Health Sciences, 1-18-1 Kamiyohga, Setagayaku, Tokyo 158-8501, Japan; e-mail: tohru@nihs.go.jp

[1]Abbreviations: BM, bone marrow; KO, knockout; UV, ultraviolet; BUUV, incorporation of bromodeoxyuridine followed by ultraviolet-light cytocide to evaluate the hemopoietic stem/progenitor cell kinetics in vivo; AhR, aryl hydrocarbon receptor; $AhR^{+/+}$, AhR wild-type; $AhR^{+/-}$, AhR heterozygous-deficient; $AhR^{-/-}$, AhR homozygous-deficient; CFU-GM, granulo-macrophage colony forming unit; CYP, cytochrome P450; FGF, fibroblast growth factor; TGF, tumor growth factor; I.V., intravenous; I.P., intraperitoneal; aft, after; dur, during; expos, exposure.

Benzene-induced leukemia is unique in that it has been associated only with a weak mutagenicity in the benzene metabolites, phenol and hydroquinone. Another interesting observation is the controversial experimental data concerning the level of actively cycling hematopoietic cells following benzene exposure. While all researchers observed a decrease in peripheral blood and BM cellularities, some observed a suppression of the cell cycle of BM, as measured by tritiated thymidine incorporation (Moeschlin and Speck, 1967), whereas others observed a marked increase in the number of cycling stem/progenitor cells in BM and peripheral blood (Table 1). Careful analysis of these apparently conflicting data revealed an enhancement of the cell cycle occurring at least 2 hours after the termination of benzene exposure. Thus, the higher tritiated thymidine incorporation documented by Cronkite et al. (1982) 18 hours after the termination of benzene exposure probably reflects a recovery phase. Based on these findings, we conducted a series of studies since 1997 to elucidate the leukemogenic effect of benzene in wild-type mice.

The *p53*-knockout (KO) mouse (Tsukada et al., 1993) showed further unique characteristics of benzene-induced leukemia. Using *p53*-KO mouse, we confirmed that benzene has a moderate genotoxic effect, as measured by the micronucleus test performed 4 weeks after the initiation of benzene inhalation (Kawasaki et al., 2001; Li et al., 2003). Moreover, *p53*-deficient mice manifest increased susceptibility to

TABLE 1.—Summary of the results the hemopoietic stem/progenitor cell kinetics during and after benzene exposure by tritiated thymidine (^{3}H-TdR) cytocide assay.

				Evaluation cell and assay methods					
		Cellularity		BM cells			CFU		
Year	Reference	Blood	BM	Kinetics	Labeling*,1	Label point	Kinetics	Labeling	Label point
1967	Moeschlin and Speck	↓	↓	↓	In vivo	At pancytopenia	—	—	—
1979	Irons et al.	↓	↓	↑	In vivo[2]	6 days aft. expos-IP	—	—	—
1982	Cronkite et al.	↓	↓	—	—	—	↑	In vitro	18 h aft. expos.
1998	Lee et al.	↓	↓	↓	In vivo[3]	30 min aft. single IP	—	—	—
		↓	↓	↓	In vitro	Dur. and aft. expos.	—	—	—
1997	Farris et al.	↓	↓	→↓	In vivo[4]	Soon aft. expos.	↑	In vitro	2 h aft. expos.

1. ^{3}H-TdR was injected intravenous (IV) at in vivo labeling except indications.
2. ^{3}H-TdR was injected intraperitoneal (IP) 6 days after cessation of benzene.
3. Benzene was treated single IP, and ^{3}H-TdR label was starting 30 minutes after benzene treatment.
4. Instead of ^{3}H-TdR, BrdUrd was used for assay.

benzene-induced leukemogenicity (Kawasaki et al., 2001). Similar findings with regard to increased leukemogenicity following benzene exposure have been documented by French et al. of the National Institute of Environmental Health Sciences (French et al., 2001). Contrary to the result in *p53*-KO mice, benzene-induced leukemia had not been detected in earlier studies in wild-type mice because its manifestations had been masked either by pancytopenia due to severe myelosuppression or by the use of a benzene dose too low to induce pancytopenia or leukemia (Kawasaki et al., 2001). Aryl hydrocarbon receptor (AhR)-KO mice (Mimura et al., 1997) also elucidated the characteristic underlying mechanism of benzene-induced hematotoxicity (Yoon et al., 2002).

In the mechanism underlying benzene toxicity in BM tissue analyzed using a microarray system, various signaling pathways have been suggested to be implicated including cell cycle regulation, DNA-damage/repair-related genes, oxidative-stress-related genes, growth-factor-related genes, oncogenes, and hemopoiesis-related genes in general (Yoon et al., 2003).

OSCILLATORY CHANGES IN BONE MARROW CELLULARITY IN WILD-TYPE MICE

BM cellularity decreases markedly during benzene inhalation but recovers rapidly following the termination of benzene exposure (Yoon et al., 2001). The oscillatory nature of the resultant curve is comparable to the response reported by Cronkite et al. (1984, 1989), and suggests that benzene does not only induce BM cell suppression but also activates cell-cycle-regulating genes, resulting in compensatory myelopoiesis.

We used the BUUV (bromodeoxyuridine + UV exposure) method to study stem/progenitor cell kinetics during or after benzene exposure (Hirabayashi et al., 1998; Yoon et al., 2001). Using this method, we were able to measure the labeling rate, cycling fraction of clonogenic progenitor cells, and other cell cycle parameters. Interestingly, the cycling fraction of stem/progenitor cells was found not to turn into active hematopoiesis but to remain low during benzene inhalation. Furthermore, rapid recovery was observed after benzene inhalation was terminated (Figure 1). However, although the exact mechanism of this phenomenon is not yet known, we found the evidence that the cycling fraction depression may be mediated in part by the suppression of stem/progenitor cell cycling per se, owing to the *p53*-dependent upregulation of p21 (Yoon et al., 2001). Thus, the mechanism of benzene-induced leukemia in the wild-type mice may be due to continuous oscillatory changes in hemopoiesis during and after the benzene exposure, which leads to genetic instability followed by the consequent epigenetic leukemogenicity.

p53-DEFICIENT MICE DEVELOP LEUKEMIA BY DIFFERENT MECHANISMS

Leukemogenicity induced in *p53*-KO mice, because of the lack of the *p53* gene, results in the noninduction of p21 expression even during the benzene exposure, with subsequent insufficient DNA repair and accumulation of DNA damage. These pathways are shown in Figure 2 for benzene-induced possible toxicological changes in both wild-type and *p53*-KO mice. In *p53*-KO mice, cell cycle suppression, DNA repair, and apoptosis of damaged cells, which, in general, occur in the wild-type mice after benzene exposure, are all suppressed. This is much more likely genotoxic leukemogenesis, in which reactive oxygen species, dysfunction of topoisomerase, and covalent binding of adduct formation to DNA,

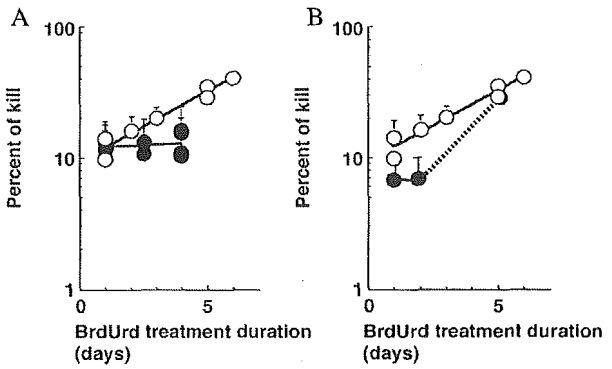

FIGURE 1.—Hemopoietic progenitor cell (CFU-GM) kinetics during (A) and after (B) benzene inhalation. Open circle: sham; Closed circle: during or after inhalation of 300 ppm benzene, 6 h/day, 5 days/week ×2 weeks. (A) For the benzene-treated group, all the mice were sacrificed just after the 5th day of the 2nd week of benzene-inhalation. The osmotic minipump filled with BrdUrd was implanted into donor mice day(s) before sacrificing as indicated on the abscissa. (B) For the benzene-treated group, the BrdUrd-pump was implanted into donor mice after the 5th day of the 2nd week of benzene-inhalation and sacrificed on the day as indicated on the abscissa. Each point represents at least 2 mice as a donor for the CFU-GM assay, and colony assays were performed in triplicate.

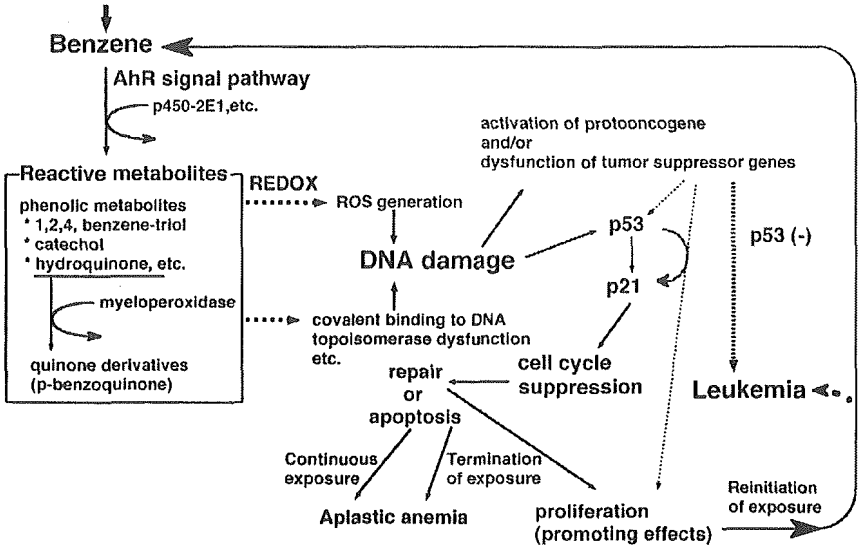

FIGURE 2.—Benzene metabolism and possible mechanism of benzene-induced leukemogenesis.

all synergistically participate in further leukemogenic development without repairing the system (see Figure 2). Thus, leukemogenicity seems to be clearly different between the mice carrying wild-type *p53* and the mice lacking *p53* (Yoon et al., 2001; Hirabayashi et al., 2002).

ARYLHYDROCARBON-RECEPTOR-MEDIATED BENZENE METABOLISM

We investigated the involvement of the aryl hydrocarbon receptor (AhR), a ligand-activated basic helix-loop-helix transcription factor, in hematotoxicity using AhR wild-type ($AhR^{+/+}$), heterozygous-KO ($AhR^{+/-}$) and homozygous-KO ($AhR^{-/-}$) male mice (Mimura et al., 1997; Yoon et al., 2002). Following a 2-week inhalation of benzene at 300 ppm, we evaluated the changes in cellularity of the peripheral blood and BM, and the levels of granulocyte-macrophage colony-forming units (CFU-GM) in the BM (Figure 3). The expression of the cyclin-dependent kinase inhibitor, p21, in BM cells and cytochrome P450 (CYP) 2E1 in hepatic tissues were evaluated by Western blot analysis after benzene exposure. Our results clearly showed that $AhR^{-/-}$ mice are much more resistant to the benzene-induced hematotoxicity than $AhR^{+/+}$ wild-type mice. No changes in p21 expression level by BM cells were detected in $AhR^{-/-}$ mice, whereas a marked up-regulation of p21 expression by BM cells was observed in $AhR^{+/+}$ mice. This finding is a further proof of the resistance of $AhR^{-/-}$ mice to benzene-induced hematotoxicity. The benzene resistance of $AhR^{-/-}$ mice was abrogated by exposure to a combination of 2 major metabolites, phenol and hydroquinone, strongly supporting the notion that AhR participates in benzene metabolism. CYP species involved in such metabolism are under investigation. The results obtained imply that pollutants that react with AhR confer marked susceptibility to benzene-induced hematotoxicity.

IMPLICATION OF MICROARRAY ANALYSIS

In the mechanism underlying benzene toxicity in BM tissue, various signaling pathways have been suggested to be implicated including metabolism, genotoxicity, cell cycle regulation, and apoptosis (Table 2). Our microarray analysis

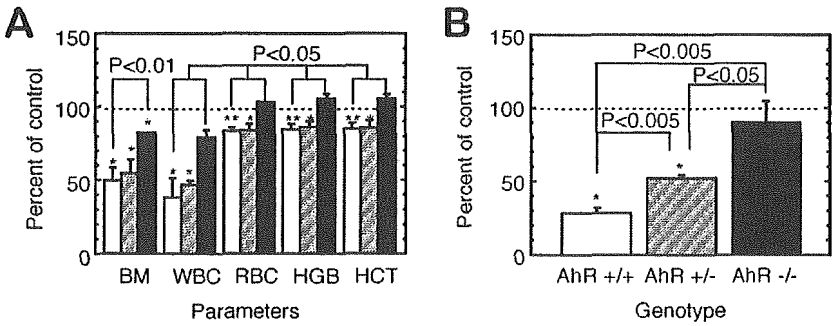

FIGURE 3.—Changes in peripheral blood parameters and BM cellularity (A) and CFU-GM per 2 femurs (B) in the AhR wild-type ($AhR^{+/+}$:open bar), heterozygous-KO ($AhR^{+/-}$:shaded bar) and homozygous-KO mice ($AhR^{-/-}$:closed bar) exposed to 300 ppm benzene for 2 weeks. The mean BM cellularities for the $AhR^{+/+}$, $AhR^{+/-}$, and $AhR^{-/-}$ mice were 4.8, 5.6, and 4.8 $\times$ 10^7/2 femurs, respectively, and the mean numbers of CFU-GM's per 8 $\times$ 10^4 BM cells was 79, 78, and 72, respectively. *, **: Significantly different from each corresponding control group at $p < 0.05$ and $p < 0.01$, respectively.

TABLE 2.—Reported genes whose expression changed during and/or after benzene inhalation.

Category	Gene name	Reference
Metabolic enzyme	CYP 2E1	Zhang et al., 2002
	Myeloperoxidase	Schattenberg et al., 1994
Cell cycle	*p53*	Boley et al., 2002
	p21 (waf 1)	
	Cyclin G	
	Gadd 45	
Apoptosis	Bax-alpha	Boley et al., 2002
Oncogene	c-fos	Ho and Witz, 1997

elucidated the up- or downregulation of genes functioning after 2-week exposure to 300 ppm benzene (Table 3): First, among cell-cycle-related genes, in addition to *p53* and p21 which are known to be upregulated to various extents depending upon the time course and the detection methods, Rb-related genes, such as the Rb-related protein p130 and the Rb-binding protein p48 are significantly upregulated; furthermore, elongation factor 1-delta shows a high expression level associated with the G2/M cell cycle checkpoint; vice versa, a significant downregulation of cyclin D1 and BimB is also recognized. Less significant changes in expression of cyclin G and Gadd45 are noted as previously reported. Second, among DNA-damage/repair-related genes, those encoding ADP-ribosylation factor-like protein 1 and Rad51 are significantly upregulated. The altered expression of other genes in the same category such as Metaxin, ERCC-3, and the DTR111 precursor are also noted, although *p*-values are not statistically significant. Third, among oxidative-stress-related genes, mitogen-activated protein kinase 2, which responds primarily to stress and inflammatory stimuli, is significantly upregulated, and the known typical ROS absorber genes, such as those encoding GST-1 and UDP glucuronosyltransferase show mild but significant increases. C3h-dioxin-inducible cytosolic aldehyde dehydrogenase-3, Cytochrome c oxidase Vb, and lactate dehydrogenase are also upregulated. Fourth, among growth-factor-related genes, those encoding the hepatocyte-growth factor-like protein shows significant upregulation, associated with a slight increase/decrease in expression level, with less significant *p*-values, for the following genes: fibroblast growth factor (FGF)-15, FGF-b, G protein-coupled receptor, growth factor-induced delayed-early-response protein, insulin-like growth factor 1 receptor precursor, insulin-induced growth response protein cl-6, tumor growth factor (TGF)-beta 1, TGF-beta 1 masking protein, and tumor necrosis factor alpha. Fifth, among the gene expression profiling of oncogenes, RhoB, which is possibly related to the genotoxic effect of benzene metabolites, shows a high expression level. Finally, hemopoiesis-related genes also show particular changes in their expression level, but the profiling of such genes led to the elucidation that benzene generally induces suppression of cell proliferation without an increase in cytokine gene expression levels.

It is of interest to determine gene expression in *p53*-KO mice with or without exposure by benzene inhalation (Yoon et al., 2003). In Table 3, the annotated genes were all downregulated (top) or upregulated (bottom) after benzene exposure, although their expressions were not altered in the wild-type mice, implying that the expressions of these genes are masked by the homeostasis governed by *p53* gene regulation. Thus, this study on *p53*-KO mice led to the elucidation of hidden gene alterations in wild-type mice, which we do not generally observe in toxicological examination.

TABLE 3.—*p53*-related genes whose expression level decreased or increased by benzene exposure, but unchanged in the wild-type mice.

WT: unchanged *p53*-KO: decreased	CalDAG-GEFI, Cbfa2, Dctn1, Frl, Grl-1, Ig/EBP, Klra3, Mek5, MEP, Mlp1, B-myb, Nog, PBX2, Prkm3, PTPalpha, Rad50, Rad51, Zfp94
WT: unchanged *p53*-KO: increased	24p3, 4E-BP2, Abcg2, ACRP, Activine, Ahd3, Alp, Anx3, AOE372, Apaf1, BAG-1, BAP, bcl-2, Calcyclin, Canexin, Caspase 9, Caspase 9S, CCR1, CD3 theta, CD71, CD143, Cox5b, Cox7a1, COX8H, Ctla-2a, Cu/Zn-SOD, Cyclin B1, DCIR, Dnmt2, Dpagt2, E4BP4, EPO, FACS, Fes, elk1, G6PD, G6PD-2, Galbp, Gapdh, Gcdh, Gdi2, Growth hormone, Gnb-1, Gng3lg, H-2T18, HES-1, IGF-1, IL1bc, IL-4, IL-9, JSR1, LDH-1, LDH-2, mLigl, Lipo 1, Lrf, Ly-3, Ly-40, Jam, JNK2, Kcc1, KSR1, M-CSF, Mac-1 alpha, Mch6, Mg11, MHR23A, MmCEN3, Mrad17, MRP14, Mtx2, NFATp, NL, Nmo1, OERK, PAFR, Pde8, PERK, PGRP, Pla2g2c, PLGF, Pop2, Prkm9, Prtn3, RBP-L, Rga, S100A13, Siva, Smad 6, SPRR2J, Stat4, Stat 5B, TCF4, TOM1, Trypsin 2, Tst

See reference, Yoon et al. (2003).

REFERENCES

Boley, S. E., Wong, V. A., French, J. E., and Recio, L. (2002). *p53* heterozygosity alters the mRNA expression of *p53* target genes in the bone marrow in response to inhaled benzene. *Toxicol Sci* **66**, 209–15.

Cronkite, E. P., Bullis, J., Inoue, T., and Drew, R. T. (1984). Benzene inhalation produces leukemia in mice. *Toxicol Appl Pharmacol* **75**, 358–61.

Cronkite, E. P., Drew, R. T., Inoue, T., Hirabayashi, Y., and Bullis, E. (1989). Hematotoxicity and carcinogenicity of inhaled benzene. *Environ Health Perspect* **82**, 97–108.

Cronkite, E. P., Inoue, T., Carsten, A. L., Miller, M. E., Bullis, J. E., and Drew, R. T. (1982). Effects of benzene inhalation on murine pluripotent stem cells. *J Toxicol Environ Health* **9**, 411–21.

Farris, G. M., Robinson, S. N., Gaido, K. W., Wong, B. A., Wong, V. A., Hahn, W. P., and Shah, R. S. (1997). Benzene-induced hematotoxicity and bone marrow compensation in B6C3F1 mice. *Fundam Appl Toxicol* **36**, 119–29.

French, J. E., Lacks, G. D., Trempus, C., Dunnick, J. K., Foley, J., Mahler, J., Tice, R. R., and Tennant, R. W. (2001). Loss of heterozygosity frequency at the *Trp53* locus in *p53*-deficient (+/−) mouse tumors is carcinogen- and tissue-dependent. *Carcinogenesis* **22**, 99–106.

Hirabayashi, Y., Matsumura, T., Matsuda, M., Kuramoto, K., Motoyoshi, K., Yoshida, K., Sasaki, H., and Inoue, T. (1998). Cell kinetics of hemopoietic colony-forming units in spleen (CFU-S) in young and old mice. *Mech Ageing Dev* **101**, 221–31.

Hirabayashi, Y., Yoon, B. I., Kawasaki, Y., Li, G. X., Kanno, J., and Inoue, T. (2002). On the mechanistic differences of benzene-induced leukemogenesis between wild type and *p53* knockout mice. *Molecular Mechanisms for Radiation-Induced Cellular Response and Cancer Development* (K. Tanaka, T. Takabatake, K. Fujikawa, T. Matsumoto, and F. Sado, eds.), pp. 110–16. Aomori, Institute for Environmental Sciences, Japan.

Ho, T. Y., and Witz, G. (1997). Increased gene expression in human promyeloid leukemia cells exposed to trans, trans-muconaldehyde, a hematotoxic benzene metabolite. *Carcinogenesis* **18**, 739–44.

Irons, R. D., Heck, H., Moore, B. J., and Muirhead, K. A. (1979). Effects of short-term benzene administration on bone marrow cell cycle kinetics in the rat. *Toxicol Appl Pharmacol* **51**, 399–409.

Kawasaki, Y., Hirabayashi, Y., Yoon, B. I., Huo, Y., Kaneko, T., Kurokawa, Y., and Inoue, T. (2001). Benzene inhalation induced an early onset and a high incidence of leukemias in the *p53* deficient C57BL/6 mice. *Jpn J Cancer Res* **92**(Suppl), 71.

Lee, E. W., Garner, C. D., and Johnson, J. T. (1988). A proposed role played by benzene itself in the induction of acute cytopenia: inhibition of DNA synthesis. *Res Commun Chem Pathol Pharmacol* **60**, 27–46.

Le Noir and Claude (1897). Sur un cas de purpura atribué a l'intoxication par la benzine. *Bull Med Soc Hop Paris* **14**, 1251–60.

Li, G. X., Hirabayashi, Y., Yoon, B. I., Kawasaki, Y., Kurokawa, Y., Yodoi, J., Kanno, J., and Inoue, T. (2003). Benzene-induced leukemia is prevented by over-expression of Trx/ADF, along with increase in Trx/ADF-expression, increase in SOD-activity, and decrease in micronuclei. *Cancer Science* **94**(suppl), 265.

Mimura, J., Yamashita, K., Nakamura, K., Morita, M., Takagi, T. N., Nakao, K., Ema, M., Sogawa, K., Yasuda, M., Katsuki, M., and Fujii-Kuriyama, Y. (1997). Loss of teratogenic response to 2,3,7,8-tetrachlorodibenzo-*p*-dioxin (TCDD) in mice lacking the Ah (dioxin) receptor. *Genes Cells* **2**, 645–54.

Moeschlin, S., and Speck, B. (1967). Experimental studies on the mechanism of action of benzene on the bone marrow (radioautographic studies using 3H-thymidine). *Acta Haematol* **38**, 104–11.

Schattenberg, D. G., Stillman, W. S., Gruntmeir, J. J., Helm, K. M., Irons, R. D., and Ross, D. (1994). Peroxidase activity in murine and human hematopoietic progenitor cells: potential relevance to benzene-induced toxicity. *Mol Pharmacol* **46**, 346–51.

Snyder, C. A., Goldstein, B. D., Sellakumar, A. R., Bromberg, I., Laskin, S., and Albert, R. E. (1980). The inhalation toxicology of benzene: incidence of hematopoietic neoplasms and hematotoxicity in ARK/J and C57BL/6J mice. *Toxicol Appl Pharmacol* **54**, 323–31.

Tsukada, T., Tomooka, Y., Takai, S., Ueda, Y., Nishikawa, S., Yagi, T., Tokunaga, T., Takeda, N., Suda, Y., Abe, S., Matsuo, I., Ikawa, Y., and Aizawa, S. (1993). Enhanced proliferative potential in culture of cells from *p53*-deficient mice. *Oncogene* **8**, 3313–22.

Yoon, B. I., Hirabayashi, Y., Kawasaki, Y., Kodama, Y., Kaneko, T., Kim, D. Y., and Inoue, T. (2001). Mechanism of action of benzene toxicity: cell cycle suppression in hemopoietic progenitor cells (CFU-GM). *Exp Hematol* **29**, 278–85.

Yoon, B. I., Hirabayashi, Y., Kawasaki, Y., Kodama, Y., Kaneko, T., Kanno, J., Kim, D. Y., Fujii-Kuriyama, Y., and Inoue, T. (2002). Aryl hydrocarbon receptor mediates benzene-induced hematotoxicity. *Toxicol Sci* **70**, 150–6.

Yoon, B. I., Li, G. X., Kitada, K., Kawasaki, Y., Igarashi, K., Kodama, Y., Inoue, T., Kobayashi, K., Kanno, J., Kim, D. Y., and Hirabayashi, Y. (2003). Mechanisms of benzene-induced hematotoxicity and leukemogenicity: cDNA microarray analyses using mouse bone marrow tissue. *Environ Health Perspect* **111**, 1411–20.

Zhang, S., Cawley, G. F., Eyer, C. S., and Backes, W. L. (2002). Altered ethylbenzene-mediated hepatic CYP2E1 expression in growth hormone-deficient dwarf rats. *Toxicol Appl Pharmacol* **179**, 74–82.